Chapter 2
The Role of the Actin Cytoskeleton in Mechanosensation

Tianzhi Luo and Douglas N. Robinson

Abstract Cells are capable of sensing mechanical stimuli and translating them into biochemical signals. This ability allows cells to adapt to their physical surroundings by remodeling their cytoskeleton, activating various signaling pathways, and changing their gene expression. These phenomena involve two essential processes – mechanosensing and mechanotransduction. In these processes, force or deformation needs to be transmitted from the outside environment to the proteins and organelles inside the cell. The actin cytoskeleton composed of actin filaments, myosin motors, and actin crosslinking proteins plays a critical role in force propagation and in response to deformations. Cellular adaptation to these deformations is often associated with feedback loops, and proteins in the actin cytoskeleton accumulate and function cooperatively in response to mechanical stimuli. Mutations in these proteins cause failure in cellular mechanosensing, which eventually leads to cellular errors associated with disease progression.

Keywords Mechanosensing · Mechanotransduction · Actin cytoskeleton · Actin-crosslinking proteins · Myosin II

2.1 Introduction

A mechanotransduction system requires at least one sensor and one transducer. The sensors, commonly located next to the outer layer of the cell membrane,

D.N. Robinson (✉)
Department of Cell Biology, Department of Pharmacology and Molecular Science, Johns Hopkins University School of Medicine, 725 N. Wolfe Street, Baltimore, MD 21205, USA; Department of Chemical and Biomolecular Engineering, Johns Hopkins University Whiting School of Engineering, 3400 N. Charles St, Baltimore, MD 21218, USA
e-mail: dnr@jhmi.edu

A. Kamkin, I. Kiseleva (eds.), *Mechanosensitivity and Mechanotransduction*, Mechanosensitivity in Cells and Tissues 4, DOI 10.1007/978-90-481-9881-8_2,

sense the mechanical stimuli, such as force, pressure and flow speed, and transmit the mechanical signals into the inside of cells. Ion channels, protein kinases, integrins, membrane glycocalyx, G proteins, intercellular junction proteins and other membrane-associated signal-transduction molecules are capable of sensing mechanical stimuli as shown in Fig. 2.1 (Ingber, 2006; Vogel and Sheetz, 2006; Wang et al., 2009). The transducers, mainly situated inside the cell membrane or inside the cytosol, convert the mechanical signals to chemical and biological signals.

Physiological examples of mechanosensation include hearing (Fettiplace and Hackney, 2006), blood flow regulation in the circulatory system (Chien, 2007), and bone remodeling (Robling et al., 2006). Auditory sensing occurs in the inner ear in a region known as the cochlea that is covered with hair cells characterized by stereocilia. The mechanoelectrical transduction (MET) ion channels in one stereocilium are linked to a neighboring stereocilium through tip linkers. These linkages are then coupled internally to the core actin bundles through myosin I motors. When one stereocilium is flexed due to sound vibrations, this induces tension along the tip link, leading to channel opening and conversion of the sound into an electrical signal. Subsequent adaption and associated closing of the METs occurs partially through the unbinding of myosin I from the actin bundles. In the circulatory system, endothelial cells sense the shear and stretch forces due to blood flow and activate a number of mechanosensors, such as membrane proteins, integrins, G proteins and ion channels. The mechanosensing triggers a cascade of signaling pathways and consequently modulates gene expression, resulting in cytoskeleton remodeling and cell realignment. Bone adapts its structure to mechanical stimuli and repairs structural damage through remodeling. At bone surfaces, osteoclasts and osteoblasts control the bone resorption and formation, respectively. However, the osteocytes, which are embedded deep within the bone, appear to have the primary

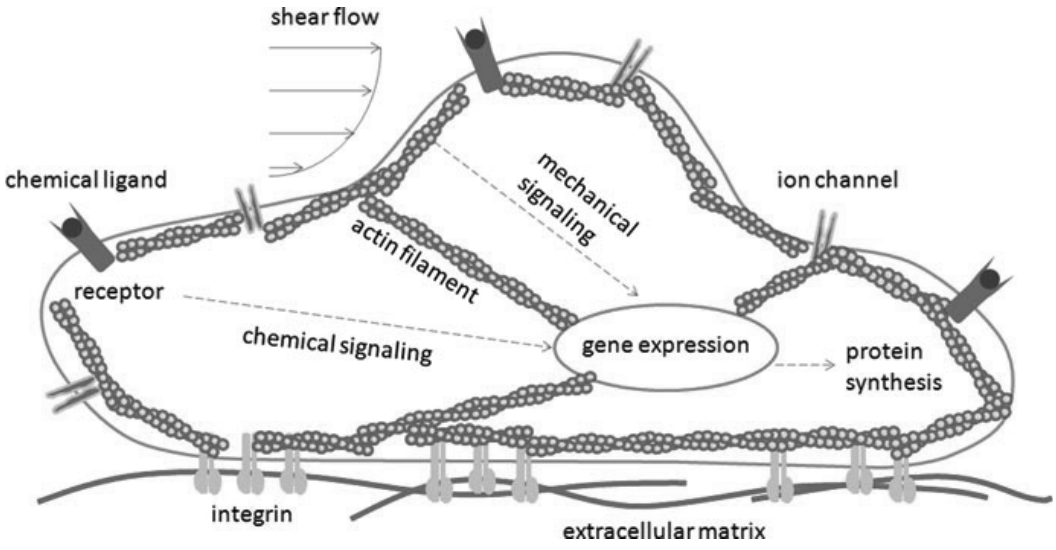

Fig. 2.1 Schematic cartoon of mechanosensation and mechanotransduction in cells

job of sensing where the bone needs to be remodeled and then relaying this information to the osteoblasts and osteoclasts located on the bone surface. One appealing model suggests that the osteocytes sense changes in fluid flow inside canaliculi and the associated viscous drag creates tensile forces along the central actin filament bundle in the osteocytes. The osteocytes then release second messengers such as prostaglandins and nitric oxide, which activate the osteoblasts and osteoclasts. At the molecular level, the bone mechanotransduction is also thought to involve ion channels, focal adhesions, and G protein-coupled receptors, but detailed molecular mechanisms are still unclear.

The actin cytoskeleton composed of actin filaments, actin crosslinking proteins (ACLPs) and myosin II motors, is unambiguously involved in these mechanosensing processes. To understand how mechanical stimuli are propagated through actin filaments and how the actin cytoskeleton responds to these stimuli, it is essential to understand the mechanical behaviors of the individual players, the reconstituted networks in vitro and the whole network in vivo.

2.2 Microstructures and Deformations of the Actin Cytoskeleton

Cellular mechanics originate from mechanical features of the cytoskeleton that traverse many length- and time-scales. On the molecular level, the mechanical properties of proteins are determined by their molecular structures, such as peptide sequences, folding states and assembly states. On the next complexity level, the mechanical properties of the actin network depend not only on its morphology/microstructures, such as mesh size, filament length, bundle diameter and homogeneity, but also on the binding strength between the actin filaments and different crosslinkers and motor activities. In the past few decades, tremendous effort has been invested in characterizing the mechanical behaviors of ACLPs and motor proteins using single molecule techniques, and many attempts have also been made to study the mechanical properties of reconstituted actin networks. However, the understanding of individual ACLPs is still far from complete due to the complexity of these proteins and the limitations of the techniques. Additionally, the mechanical strength of reconstituted actin networks are often several orders lower than that of the intact cells.

The central core protein of the actin cytoskeleton is monomeric actin, a 5-nm diameter, 42 kDa globular protein (G-actin) found in all eukaryotic cells. Each monomer is organized into four subdomains, flanking an internal cleft that binds ATP and magnesium ions. The end of G-actin close to the base of the cleft is called the plus end and the opposite end is called the minus end. G-actin monomers undergo polymerization and form microfilaments (F-actin) upon the addition of salt. Since the plus end of one G-actin is connected to the minus end of the neighboring G-actin, microfilaments also have well-defined plus and minus ends. The inclusion of ATP assists in G-actin stability and dramatically reduces the critical concentration for assembly. The 8-nm wide actin filament can be considered to have a left-handed

helical morphology with 13 actin monomers per pseudo-repeat and a pseudo-repeat length of 37 nm. Alternatively, the actin filament can be considered to have a right-handed helical structure with two strands slowly twisting around each other. Each actin monomer is rotated 166° rotation with respect to its two nearest neighbors across the strand (Holmes et al., 1990). Within the strand, subdomains 2 and 4 contact subdomains 1 and 3 in the next monomer in the strand, and each monomer reaches across to the other strand through a hydrophobic plug that links the two strands together. The persistence length L_p of pure F-actin is around 17 μm. The intrinsic bending stiffness, $\kappa_b = L_p k_B T$, and the elastic Young's modulus E are 7×10^{-26} N·m^{-2}and 2.6×10^9 N·m^{-2}, respectively (Gittes et al., 1993; Kojima et al., 1994). The effective stretching stiffness is 44 pN·nm^{-1} provided the cross-sectional area of a fully filled filament is 25 nm^{-2}, and the torsional rigidity is 8×10^{-26} N·m^{-2} (Tsuda et al., 1996).

Non-muscle myosin II, a member of the conventional myosin II superfamily, is composed of functional hexameric monomers, consisting of two heavy chains, two essential light chains (ELCs) and two regulatory light chains (RLCs), which combine to form a ~500 kDa complex (shown in Fig. 2.2). The amino-terminal motor domain consists of the catalytic core, which is structurally conserved with the Ras-family small GTPase and includes the switch I and switch II helices and a Walker p-loop-family nucleotide-binding pocket. This catalytic core is functionalized with an actin-binding interface and a converter domain. The converter domain connects to an 8-nm long α-helix, which is wrapped by an ELC and RLC, forming the lever arm. The lever arm links to the carboxyl-terminal coiled coil domain (Warrick et al., 1987). Upon binding to actin, the motor domain remains rigid, whereas the lever domain is rotated through a ~70° angle as the products of ATP hydrolysis are released; this lever arm rotation leads to the translation of the actin filament relative to the coiled coil of the myosin.

To generate force and to bear load, myosin II must assemble into bipolar thick filaments (BTFs). These assemblies can range from as few as eight (*Acanthamoeba*)

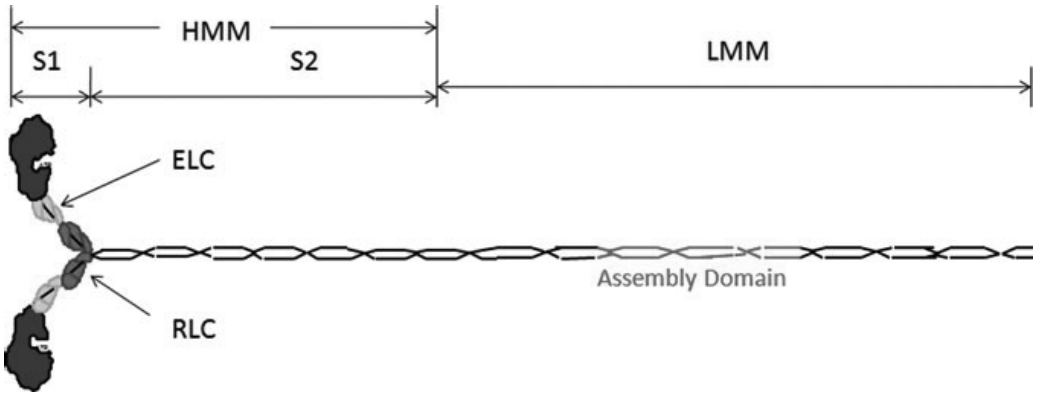

Fig. 2.2 Domain structure of myosin II. HMM and LMM represent heavy meromyosin and light meromyosin, respectively

to as many as 400 hexamers (mammalian skeletal muscle). Most mammalian nonmuscle myosin IIs (nonmuscle heavy chain IIA, IIB and IIC) assemble into BTFs ranging from 10–30 monomers, and *Dictyostelium discoideum* myosin II is thought to assemble into BTFs with up to 70 monomers. For *Dictyostelium*, the assembly process is thought to occur through the formation of two monomers into a parallel dimer and two of these parallel dimers join together to create an anti-parallel tetramer. Once the anti-parallel tetramer is formed (the stable nucleus), the BTF grows through side-by-side (lateral) addition of dimers, resulting in no extra elongation of the BTF as more dimers are added (Fig. 2.3) (Mahajan and Pardee, 1996). In the thick filament, myosin II molecules are thought to stack their rod tails in parallel with a small overlap where the subunits are held together through electrostatic interactions (Hostetter et al., 2004). Therefore, unlike muscle myosin II thick filaments which grow in length as they are assembled, the *Dictyostelium* myosin monomer is 250 nm whereas the thick filaments are just 400 nm long, independent of the number of monomers assembled. The assembly process is regulated by myosin heavy chain kinases (MHCKs), which phosphorylate three critical threonines in the tail region (Liang et al., 1999). This phosphorylation prevents the myosin monomer from assembling into BTFs, which is necessary to maintain a free pool (80–90% of total myosin II) of monomeric myosin in the *Dictyostelium* cell.

ACLPs can organize actin filaments into bundles and branched networks, depending on their molecular structures (as shown in Fig. 2.4), kinetic properties, and concentration (Revenu et al., 2004). Bundle forming ACLPs include fascin, forked, villin, fimbrin, espin, scruin, plastin, cortexillin and dynacortin, whereas examples of meshwork forming ACLPs are filamin, Arp2/3, gelsolin and ERM (ezrin, radixin, and moesin) proteins. Some of these proteins have additional properties. For example, Arp2/3 also nucleates actin assembly and ERMs link actin filaments to the membrane. However, this classification of bundlers versus meshwork formers is an oversimplification as some ACLPs, such as α-actinin and dynacortin, can form bundles or meshworks depending on concentration and actin:crosslinker ratios. Some of these ACLPs, such as villin, espin, forked, fimbrin

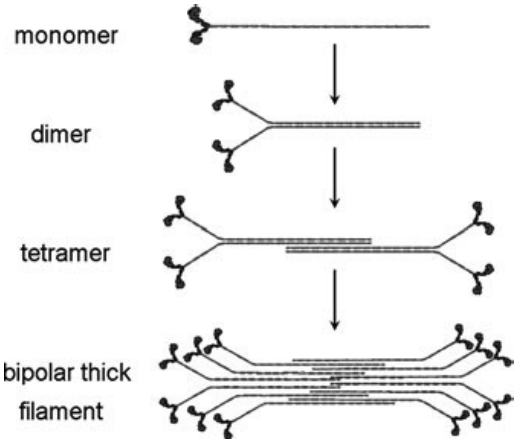

Fig. 2.3 Illustration of the assembly process of non-muscle myosin II

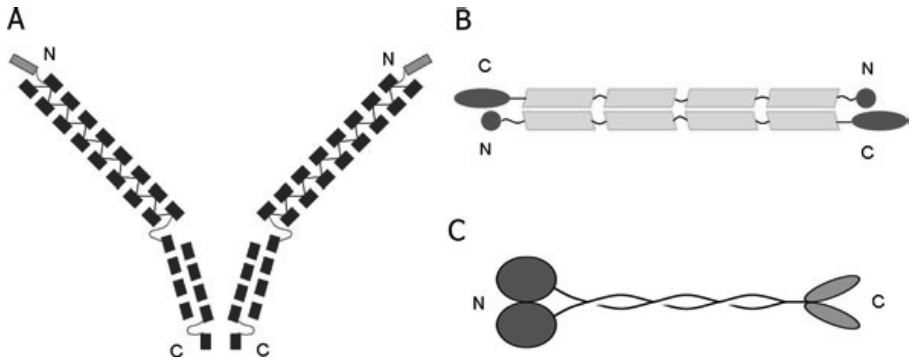

Fig. 2.4 Schematic graph of a few actin crosslinking proteins:(**a**) human filamin A; (**b**) α-actinin; (**c**) cortexillin-I. In all cases, "N" and "C" represent the N-terminus and C-terminus, respectively

and fascin, are monomeric with at least two actin-binding motifs, allowing them to crosslink as monomers. By contrast, other ACLPs, such as filamin A, α-actinin, dynacortin, and cortexillin are dimeric, and filamin A, cortexillin, and most likely dynacortin form parallel dimers while α-actinin forms anti-parallel dimers. Actin-binding domains are localized at the amino-terminus of filamin A and α-actinin. Due to the differences in their structures, Y-shaped filamin A dimers can only crosslink actin filaments into nearly orthogonal networks while α-actinin forms either networks or loose bundles. Some of the most common filamentous actin-binding domains (ABDs) are the calponin homology (CH) domain, the Wiskott-Aldrich syndrome homology region 2 (WH_2) domain, the gelsolin homology (GH) domain, and the formin homology (FH) domain (Sjöblom et al., 2008). Different ABDs generally associate with different surfaces on the actin monomer and with different apparent affinities.

These network structures may experience four types of deformations (Vogel, 2006; Ferrer et al., 2008): (1) deformation in actin filaments, (2) deformation of the binding between actin filaments and myosin-II, (3) deformation of the binding between actin filaments and ACLPs and (4) intramolecular deformation of ACLPs. In other words, intermolecular and intramolecular deformations exist at the same time within the same network. One additional feature of how these networks respond to deformation is the relationship of the time-scale of the deformation to the time-scale of the turnover/remodeling of the network. For example, profilin binds monomeric actin, inducing it to exchange its nucleotide and shuttling the actin monomer to sites where elongation has been stimulated. By contrast, cofilin binds cooperatively to sever the actin filaments, which has a complicated effect on the actin network. Severing provides free actin plus ends that may grow whereas the free minus ends can disassemble. These proteins influence the time-scales over which the actin polymers can grow and disassemble, modulating the time-scales of remodeling of the actin network. These features of network remodeling may provide a phenomenological viscous character to the network, allowing it to flow and remodel over the long time-scales of many biological processes.

2.2.1 Intermolecular and Intramolecular Deformations

Intermolecular interactions, including hydrogen bonds, electrostatic interactions, van der Waals interactions and hydrophobic interactions, are non-covalent in nature. Based on the transition state theory, there are two popular bond models to describe the single-bond behaviors of intermolecular interactions: the catch-bond model and the slip-bond model. A simplified definition of the catch-bond model is the lifetime of the bond increases as the stretching force increases. In contrast, a slip-bond shows the opposite behavior, i.e., the bond lifetime decreases as the force increases. A schematic diagram of the energy landscapes of the two different models are shown in Fig. 2.5. In the spirit of Bell (Bell, 1978), both models can be described by the unified formula (Evans and Ritchie, 1997; Evans, 2001):

$$k_{\text{off}} = k_{\text{off}}^{0} \exp\left(\frac{f\Delta x}{k_{\text{B}}T}\right), \tag{2.1}$$

where $k_{\text{off}}^{0} = \nu \exp\left(-\Delta G / k_{\text{B}}T\right)$ is the unbinding rate in the absence of force, ν is the vibration frequency, ΔG is the energy difference between the transition state and the bound state, k_{B} is Boltzmann's constant, T is temperature, f is the external force that pulls the two molecules apart, and Δx is the bond length change along

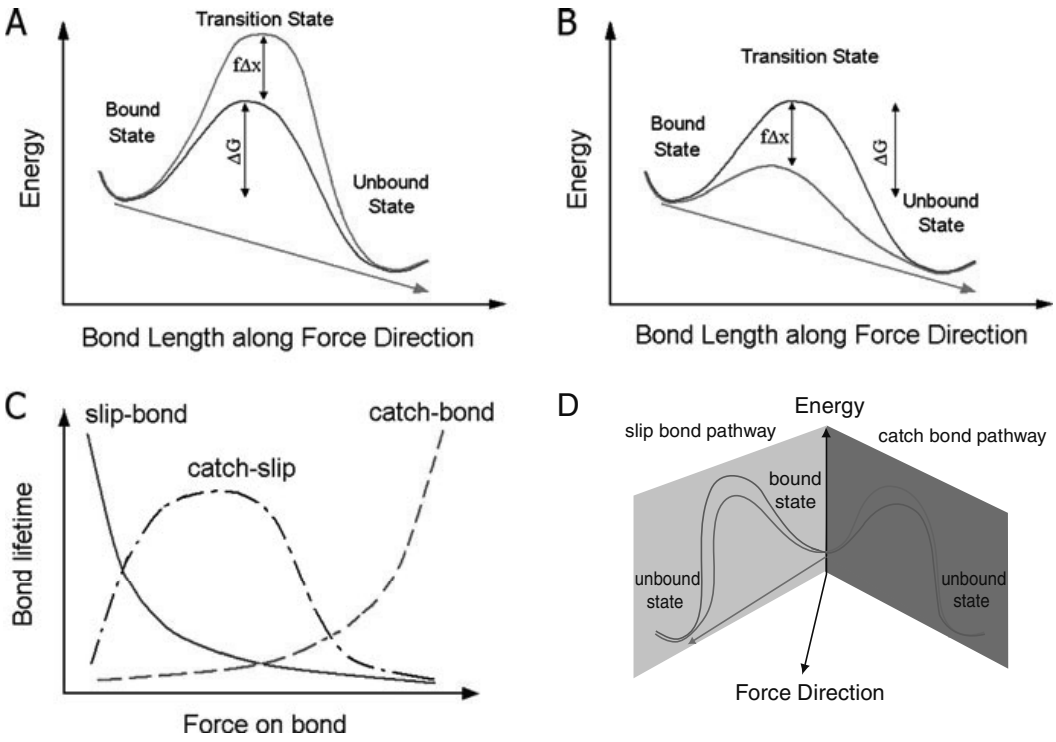

Fig. 2.5 A schematic diagram of the force dependence of protein-protein interaction strength: (**a**) catch-bond model; (**b**) slip-bond model; (**c**) three typical bond behaviors; (**d**) two pathways between bound state and unbound state. Red and blue lines are energy landscapes in the presence and absence of external load, respectively

the force direction. When the force pulls the system close to the transition state, i.e., $f\Delta x > 0$, Eq. (2.1) describes the slip-bond model; however, when $f\Delta x < 0$, it refers to the catch-bond model. Equation (2.1) can only be applied to a single pathway (either catch-bond or slip-bond). However, sometimes there are multiple pathways between the bound state and unbound state, and catch-slip and slip-catch transitions usually occur (as shown in Fig. 2.5). In that case, the unbinding rate is a superposition of the rates of two different pathways:

$$k_{\text{off}} = k_{\text{s}}^0 \exp\left(\frac{f\Delta x_{\text{s}}}{k_{\text{B}}T}\right) + k_{\text{c}}^0 \exp\left(\frac{f\Delta x_{\text{c}}}{k_{\text{B}}T}\right), \tag{2.2}$$

where the subscript s and c represent slip and catch, respectively.

To characterize intermolecular interactions, two kinds of experiments are often conducted: the measurement of the bond life-times at a constant force and the measurement of rupture forces at a constant loading speed. Under constant force conditions, the surviving probability $P(t)$ of a bond in the bound state satisfies (Thomas, 2008)

$$\frac{dP(t)}{dt} = -k_{\text{off}}(f)\,P(t), \tag{2.3}$$

where $k_{\text{off}}(f)$ is described by Eq. (2.1). Apparently, $P(t)$ decreases exponentially over time and the slope of $P(t)$ in log scale is $-k_{\text{off}}(f)$. For the slip-bond model, the surviving probability shows a larger negative slope when force increases; whereas for the catch-bond model, it shows the opposite trend. Under constant loading rate conditions, the rupture force is

$$f^* = \frac{k_{\text{B}}T}{\Delta x}\ln\left(\frac{\Delta x}{k_{\text{off}}^0 k_{\text{B}}T}\right) + \frac{k_{\text{B}}T}{\Delta x}\ln\left(r_f\right), \tag{2.4}$$

where r_f is the loading rate and $f(t) = r_f t$ (Ackbarow et al., 2007). Equation (2.4) predicts a linear relationship between the rupture force and logarithm of the constant loading rate. If the intermolecular interaction involves multiple bonds, the $f^* \sim \ln\left(r_f\right)$ will show different slopes associated with different bond energies.

Intramolecular interactions include covalent bonds, hydrogen bonds, electrostatic interactions, van der Waals interactions, and hydrophobic interactions. Mechanical deformation can cause twisting and stretching of a single bond or the whole protein, general conformational changes and the unfolding of domains. Since intramolecular interactions are much more complicated than intermolecular interactions, there is no simple mathematic model to describe how mechanical force affects the intramolecular interactions even though protein unfolding can still be probed experimentally using similar techniques. However, for a linear polyprotein, such as an actin filament and titin, the force-extension relationship can be predicted using a worm-like-chain (WLC) model that was originally developed to describe the mechanical behaviors of double stranded DNA molecules (Bustamante et al., 1994; Marko and Siggia, 1995):

$$f = \frac{k_B T}{L_p}\left[\frac{1}{4\left(1 - x/L_c\right)^2} + \frac{x}{L_c} - \frac{1}{4}\right], \tag{2.5}$$

where Lp is the persistence length, L_c is the contour length, and x is the extension. Another popular model of the force-extension of proteins is the free-joint-chain (FJC) model (Bueche, 1962):

$$x = L_c\left[\coth\left(\frac{fl}{k_B T}\right) - \frac{k_B T}{fl}\right], \tag{2.6}$$

where l is the Kuhn monomer size. In the WLC model, the force is written as a function of the chain extension while in FJC model the extension is written as a function of the force. However mathematically, both models give similar force-extension curves.

2.2.1.1 Force Generation Associated with Actin Polymerization

Actin polymerization, like microtubule polymerization, is force generating. During actin polymerization, actin monomers bound with a nucleotide assemble into helical filaments. The nucleotide binding cleft sits between subdomain 2 and subdomain 4, which faces the minus or pointed end of the actin filament. The opposite end is the fast growing so-called barbed- or plus-end of the filament. The plus and minus ends have different affinities for ADP-actin or ATP-actin monomers with the plus end having the highest overall affinity for ATP-actin monomer. After some time delay after the ATP-actin monomer incorporates into the polymer, the ATP is hydrolyzed to ADP•P_i. Subsequently, the P_i is released, leaving behind an ADP-actin monomer within the actin filament. The effect of these kinetics is that a density gradient of ATP-, ADP•P_i-, then ADP-actin monomers extends from the plus- to minus-ends of the actin polymer. In comparison to ATP-monomers, ADP-monomers have different conformations and are less stable in the filament form. Therefore, at concentrations between the critical concentrations of the two ends, net polymerization at the plus end and net depolymerization at the minus end lead to treadmilling: the net flow of actin monomers from plus end to the minus end. During polymer assembly, the filament can generate a force, measured at 1 pN, which is close to the theoretical estimate (for a given concentration of G-actin) according to

$$f = \frac{k_B T}{\delta}\ln\left(\frac{k_+ c_A}{k_-}\right), \tag{2.7}$$

where δ is the length increment of one monomer addition, $k_+(k_-)$ is the on(off) rate of polymerization at the plus end, and c_A is actin concentration (Kovar and Pollard, 2004; Footer et al., 2007). Therefore, filament assembly by itself is force generating, and compressive forces can suppress filament growth. Furthermore, the

theoretical estimate implies that simply by increasing the free actin concentration, greater forces may be generated by filament assembly. However, this process is limited by the flexural rigidity of the filament, which sets a force limit beyond which the filament buckles. However, actin-associated proteins may increase the flexural rigidity, increasing the range of forces that might be generated by filament assembly.

2.2.1.2 Force-Dependent Behaviors of Actin-Myosin Binding

Myosin II is one type of an actin-based motor that converts chemical energy into mechanical work by amplifying a small conformational change associated with ATP hydrolysis in its motor domain and translating it into the relative movement of the myosin II and the actin filament. The actin-activated myosin II ATPase cycle is shown in Fig. 2.6 (Spudich, 2001). Initially, ATP binds to the nucleotide-binding pocket in the myosin head (motor domain), which results in the unbinding of the motor from an actin filament. Upon ATP hydrolysis, the myosin rotates its lever arm, moving the head into the pre-stroke state. In this state, the motor can weakly sample the actin filament in search of its binding site. Upon binding, the motor locks on tightly and releases the P_i as the head begins to swing the lever arm through its working stroke (a $\sim 70^\circ$ rotation). Upon completing the full working stroke, the ADP-bound motor remains locked onto the actin filament. Subsequently, the motor releases the ADP, forming the so-called rigor state. ATP can then rebind, starting the cycle over again, which will continue until ATP is depleted. The time the motor spends tightly bound to the actin filament is the strongly bound state time. The ratio of the strongly bound state time to the entire ATPase cycle time gives rise to a duty ratio, which specifies the fraction of time each motor domain spends tightly bound to actin and correspondingly, the fraction of motor heads tightly bound to actin at any time. Because the motor generates force as it translates the actin filament, the

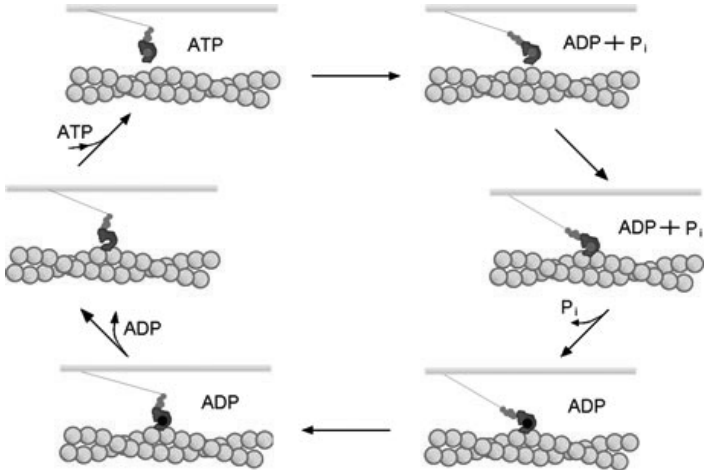

Fig. 2.6 Myosin II ATPase cycle

motor performs work as it undergoes its conformational change. For most myosin family members (with myosin VI having some unique and exquisitely complicated twists on this theme (Phichith et al., 2009)), the head region is highly rigid while the lever arm is considered to be elastic. Furthermore, the ADP-release step itself is not force-sensitive for most myosin isoforms. Rather the conformational changes that precede the formation of the ADP-bound post-stroke configuration are force-sensitive. Therefore, as the motor swings the elastic lever arm through its power stroke, resistive tension can lead to deformation (strain) of the lever arm, inhibiting the lever arm swing and locking the motor in the load-bearing, transition state. Moreover, the step-size of the myosin is related to the length of its lever arm, and this relationship has been shown to be linearly proportional to the lever arm length for *Dictyostelium* myosin II. A further hypothesis is that the maximum force depends on the length of the lever arm (Uyeda et al., 1996). Lower force is required to stall a motor with a long lever arm whereas the same motor with a short lever arm powers through greater loads before being stalled by load, implying that the strain on the lever arm prevents the full conformational change needed to allow for the motor to acquire the conformation where it can release the ADP. This load-dependency is consistent with a catch-slip-like behavior, which can be interpreted using Eq. (2.4).

2.2.1.3 Force-Dependent Binding Between Actin Crosslinkers and Actin Filaments

In order to crosslink or bundle two actin filaments, an ACLP must have a minimum of two actin-binding domains associated with each functional unit through which the ACLP contacts the actin filaments. This can occur by either dimerizing a monomer that contains one ABD or by having two or more ABDs within a monomer. Furthermore, the strength of the actin interactions and the conformation of the actin network (meshwork or bundle) varies for different ABDs and the different conformations of ABDs within the ACLP. For example, the ABDs may be closely linked through short spacers (e.g. fimbrin), resulting in tightly packed actin bundles or there can be elongated spacers (e.g. α-actinin and spectrin), which can form relatively loose networks (Bañuelos et al., 1998). The most common ABD module is composed of two tandem CH domains; this module is found in ACLPs such as α-actinin, spectrin, dystrophin, fimbrin, filamin, plectin and cortexillin. For comparison, the dissociation constants of *Acanthamoeba* α-actinin, chicken smooth muscle α-actinin and *Dictyostelium* α-actinin are 4.7, 0.6 and 3 μM, respectively even though the first two have very similar structures (Wachsstock et al., 1993). In single molecule measurements, filamin A and rabbit muscle α-actinin have actin-unbinding energies of 4.3 k_BT and 3.6 k_BT, respectively, while displaying increasing rupture forces with increasing loading rates (Ferrer et al., 2008). The loading rate dependence of the rupture forces of these crosslinkers is indicative of catch-bond behavior.

2.2.1.4 Force-Dependent Intramolecular Deformation of ACLPs

During the deformation of the actin cytoskeleton, ACLPs undergo intramolecular deformations, which involve domain unfolding and shearing and stretching between two actin-binding domains. The unfolding process can be assessed experimentally by single molecule stretching, and the resulting saw tooth-like force-extension curve usually agrees well with the WLC model. Molecular dynamics simulations can also be used to computationally pull on proteins from various directions at relatively high pulling speeds to reveal detailed unfolding schemes. The most common structures of interest typically include bundles of α-helices or β-sheets (Rohs et al., 1999; Ackbarow et al., 2007; Buehler and Keten, 2008). Two studied examples are filamin and α-actinin, both of which form anti-parallel homodimers. However, filamin is constructed from multiple β-sheet-like immunoglobulin (Ig) domains, the number of which differs between various family members. By contrast, α-actinin includes multiple spectrin repeats, each of which consists of a bundle of three α-helices. *Dictyostelium* filamin (DdFLN) consists of an ABD at the amino-terminal end followed by a rod domain, containing six Ig domains. Single molecule stretching of DdFLN revealed that the sequence of the fourth Ig domain is unique because it has a lower unfolding force (Schwaiger et al., 2004). Additionally, it was found that the fourth Ig domain has an intermediate unfolded state in the low force regime. Based on the WLC model, the persistence length is 0.5 and 0.9 nm for the high force regime and the low force regime, respectively. The corresponding unfolding force ranges from ∼50–250 pN and the periodicity of extension also ranges from ∼14–17 nm. Similarly, the human endothelial filamin A has one ABP and 24 Ig repeats plus two flexible hinges. However, despite the diversity in the structures between the two filamin family members, the force extension curve reveals a similar persistence length of 0.33 nm and an unfolding force, ranging from 50 to 200 pN (Furuike et al., 2001). The unfolding of spectrin repeats requires an unfolding force of ∼30–50 pN, a persistence length of 0.8 nm and an extension period of 31 nm (Rief et al., 1999). In the Ig domains, β-strands are arranged almost in anti-parallel fashion with small twist angles mainly through hydrogen bond interactions. During mechanical unfolding, two anti-parallel strands slide in opposite directions while breaking the hydrogen bonds between them (Lu and Schulten, 2000; Keten and Buehler, 2008). Many studies have shown that the unfolding of β-sheet proteins depends highly on the pulling directions (Brockwell et al., 2003; Nome et al., 2007; Dietz et al., 2006; Bertz et al., 2009). In each spectrin repeat, three antiparallel α-helices linked by loops are folded into a left-handed coiled coil (Pascual et al., 1997; Djinović-Carugo et al., 1999). Despite the elasticity of coiled-coil structures, the unfolding of these repeat domains mainly relies on the stretching of the linkage between different helices (Altmann et al., 2002). The linkage dependent unfolding has also been observed in other proteins (Carrion-Vazquez et al., 2003). In summary, the full force-extension relationship of individual proteins can be obtained by linear superposition of the force-extension of each domains and linkages while considering the corresponding folding and unfolding probability at certain forces (Li et al., 2002).

2.2.2 Mechanical Properties of an Actin Network

The mechanical properties of an in vitro assembled actin network depend on the average length of actin filaments, the mesh size of the actin network, the concentration of myosin II, the assembly states of myosin II thick filaments, the concentration of ACLPs, the binding strength between ACLPs and actin filaments, the mechanical properties of each ACLP and the heterogeneity of the actin network (Gardel et al., 2004a; Wagner et al., 2006; Bausch and Kroy, 2006; Ferrer et al., 2008). The addition of myosin II can alter the fundamental character of the actin network. In response to mechanical stimuli, the actomyosin system undergoes continuous remodeling of its microstructure. The remodeling of the actin-myosin II contractile system includes assembly/disassembly of actin filaments and myosin II thick filaments and bundling/unbundling of actin filaments by ACLPs. During remodeling, the whole network is more or less out of mechanical equilibrium, which leads to transient behaviors within the network (Mizuno et al., 2007; Wilhelm, 2008).

2.2.2.1 Mechanical Properties of Pure Actin Gels

Polymers can be divided into three groups based on two length scales: the persistence length L_p and the contour length L_c. A filament is considered rigid if $L_p >> L_c$ or flexible if $L_p << L_c$. Otherwise if $L_p \sim L_c$, the polymer behaves as though it is semi-flexible. In vitro, actin filaments assembled from 1-μM monomer display an exponential length distribution ranging from ~2–70 μm with a mean length of 22 μm (Kaufmann et al., 1992). It should be noted, however, that the length distribution of many in vivo networks is much smaller. For example, *Dictyostelium* cells have an actin filament length distribution that appears to be broadly distributed but with a mean length of only ~100 nm despite that the total (monomer plus polymer) actin concentration is ~250 μM (Reichl et al., 2008). Nevertheless, for the in vitro networks and the actin polymer persistence length of ~10–17 μm, the polymers are semi-flexible so that the response to deformation depends on bending and compression of the filaments. The free energy has the form

$$E = \int_0^{L_c} \left[\frac{\kappa_b}{2} \left(\nabla^2 u \right)^2 + \frac{f}{2} \left(\nabla u \right)^2 \right] dz, \tag{2.8}$$

where $u(z)$ is the transverse deviation of the filament away from a straight conformation along the z-axis (MacKintosh et al., 1995). Based on the equipartition theorem, the force-extension of a single actin filament is

$$L = L_c - \frac{L_c^2}{\pi^2 L_p} \sum_{n=1}^{\infty} \frac{f}{n^2 \left(n^2 f_b + f \right)}, \tag{2.9}$$

where $f_b = \pi^2 \kappa_b / L_c^2$ is the threshold force for the Euler buckling instability and L is the end-to-end distance. In the low force regime, the force is approximately

a linear function of extension, i.e. $f \sim k^2 (L_c - L) / (\kappa_b T L^4)$ (Storm et al., 2005). However, the force-extension relationship diverges nonlinearly as $f \sim 1/(L_c - L)^2$ in high force regimes where $L \to L_c$. Therefore, the stress increases non-linearly with increasing strain. That is the F-actin shows strain-stiffening at high stress or high strain, which is an essential property of many biological materials.

Semi-flexible polymers are viscoelastic in nature, i.e., their deformation is time-dependent (frequency-dependent) and loading-history dependent (pre-stress-dependent). The complex modulus $G^*(\omega)$ can be measured by applying an oscillatory shear strain $\gamma \sin(\omega t)$ to the actin solution and by measuring the stress $\sigma \sin(\omega t + \delta)$, where ω is the frequency and δ is the phase shift in the range of $0 \sim \pi/2$ with δ=0 and δ=$\pi/2$, corresponding to a Hookean solid and Newtonian fluid, respectively. The shear and loss moduli are defined as $G'(\omega) = |G^*(\omega)| \cos(\delta(\omega))$ and $G''(\omega) = |G^*(\omega)| \sin(\delta(\omega))$, respectively. The complex modulus of F-actin has a very weak frequency dependency in the low frequency regime 0.01–10 Hz whereas it shows a strong frequency dependency ($G^* \sim \omega^{3/4}$) in the high frequency regime (10–10,000 Hz) (Gittes et al., 1997; Gisler and Weitz, 1999; Crocker et al., 2000). The shear modulus also shows a concentration dependency in which the concentration determines the mesh size ξ of the actin network and l_e is the distance between entanglement points. The 2D density of filaments then is ξ^{-2} and $\xi \sim 0.3/\sqrt{ac_A}$, where a is the actin monomer size and c_A is the actin concentration (Schmidt et al., 1989). If the extension is assumed to be linearly proportional to l_e, then the shear modulus of the actin filament network at small strains is

$$G' = \frac{\sigma}{\gamma} \sim \frac{\kappa_b}{k_B T \xi^2 l_e^3}, \tag{2.10}$$

where σ and γ are stress and strain, respectively (MacKintosh et al., 1995). Furthermore, the fluctuating segment of length l_e occupies a volume of $k_B T L_e^4 / \kappa_b$ and the shear modulus can be written as a function of c_A such that $G' \sim \kappa_b (\kappa_b / k_b T)^{2/5} (a c_A)^{11/5}$, i.e., $G' \sim c_A^{11/5}$. On the other hand, considering the excluded volume of a filament from an entropy point of view, one expects $G' \sim c_A^{7/5}$ (Hinner et al., 1998; Gardel et al., 2003). Therefore, the moduli of actin networks have a power low dependence on actin concentration and the corresponding exponent is in the range between 7/5 and 11/5. Experiments of actin solutions with controlled filament length (Hinner et al., 1998) and uncontrolled filament length (Gardel et al., 2003) showed $G' \sim c_A^{7/5}$ and $G' \sim c_A^{9/5}$, respectively. However, this power law dependence breaks down when the thermal fluctuation of actin filaments is severely depressed. For example, in a confined volume such as a spherical aqueous droplet, the entropic effect gives $G' \sim k_b T l_p^{1/2} / D^{7/2}$ when $l_p < D$, where D is the diameter of the droplet (Claessens et al., 2006b). Therefore, the modulus is as much a function of the size of confinement as it is a function of actin concentration.

2.2.2.2 Effects of Crosslinking Proteins on the Microstructures and Mechanical Properties of Pure Actin Networks

ACLPs microstructurally crosslink actin filaments to form bundles and/or isotropic meshworks, which generally raises the shear modulus three orders of magnitude from ~0.1 Pa to ~100 Pa. In comparison to actin networks without ACLPs at a specific actin concentration, bundled actin networks have a larger mesh size and increased bending modulus for each bundle while an isotropic meshwork has a decreased mesh size. For bundled filaments, if the ACLPS are short and rigid, the bending of all of the filaments inside the same bundle is coupled and the bending modulus of each bundle shows a quadratic dependence on the number of filaments. However, if the ACLPs are long and flexible, the filaments are incompletely coupled, and the bending modulus of each bundle has a linear dependence on the number of filaments (Claessens et al., 2006a). Based on Eq. (2.10), the effects of bundling proteins are two-fold: first, they increase ξ and l_e and second, they enhance the effective bending modulus of each filament. This two-fold impact can be observed in filaments bundled by the fimbrin isoform plastin, which shows this linear dependence, while that of the bundles generated by depletion forces induced by polyethylene-glycol (PEG) displays a quadratic dependence on filament number. However, more complex relationships are also observed. The bending moduli of fascin and α-actinin bundles transition from linear to quadratic dependencies with increasing ACLP concentration. This two-phase behavior may be due to the increasing resistance to the relative shearing between two filaments during bending with increasing ACLP concentrations (Claessens et al., 2006a). To eliminate the effect of the deformation of bundling proteins, scruin (a very rigid tight-packing crosslinker) was used to bundle actin filaments. Here, $G'(\omega)$ shows a quadratic dependence on the crosslinking density ς (the ratio between the crosslinker concentration and actin concentration) and $G' \sim c_A^{2.5}$ (Gardel et al., 2004a, b). The corresponding filament bundle diameter scales as $D \sim \varsigma^{0.3}$ and $\xi \sim \varsigma^{0.2}$ as shown in Figs. 2.7 and 2.8 (Shin et al., 2004). For fascin-bundled F-actin, G' correlates strongly with the microstructures: above a critical ς, $G' \sim \varsigma^{1.5}$ and $G' \sim c_A^{2.4}$; below that, $G' \sim \varsigma^{0.1}$ and $G' \sim c_A^{1.3}$ (Lieleg et al., 2007). The corresponding bundle diameter scales as $\varsigma^{0.27}$. Similarly, engineered proteins containing different repeats in hisactophilin and disulfide bond-linked hisactophilin dimers exhibit $G' \sim \varsigma^{0.6}$ and $G' \sim \varsigma^{1.2}$, respectively (Wagner et al., 2006), which indicates that the interaction between two dimers is also very important. It was proposed that $G' \sim c_A^{11/5} \varsigma^{(6x+15y)/5}$, where x is the bundling exponent and y is the crosslinking exponent for bundled F-actin (Shin et al., 2004). $G'(\omega)$ and $G''(\omega)$ show a weak frequency dependency in the low frequency regime. However, both scruin and biotin-avidin crosslinked actin networks have $G'(\omega) \sim G''(\omega) \sim \omega^{3/4}$ in the high frequency regime (Gardel et al., 2004b; Koenderink et al., 2006). By contrast, fascin-bundled actin shows $G'(\omega) \sim G''(\omega) \sim \omega^{0.5}$ (Lieleg and Bausch, 2007). Apparently, actin networks crosslinked by scruin and biotin-avidin interactions, but not fascin, display a similar power-law dependency of the elastic modulus on frequency at these high frequencies as that of pure-actin gels.

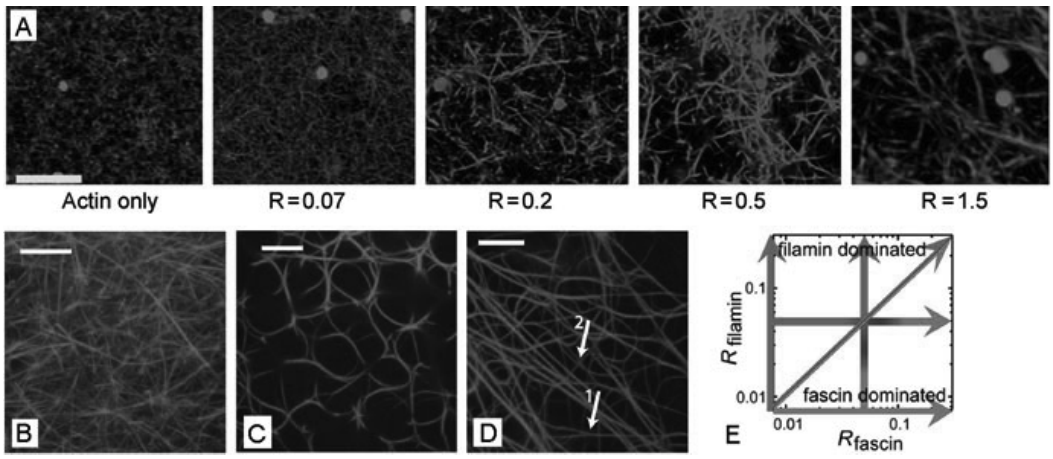

Fig. 2.7 Microstructural images of actin networks crosslinked by ACLPs seen by confocal microscopy. The actin bundle size increases with the [scruin]/[actin] ratio R as shown in **a**. Pure actin-fascin ([fascin]/[actin] = 0.05) and pure actin-filamin ([filamin]/[actin] = 0.1) are shown in **b** and **c**, respectively. **d** shows the actin composite crosslinked by fascin and filamin at [fascin]/[actin] = 0.01 and [filamin]/[actin] = 0.1. An illustration of the structural features dominated by individual ACLP when its concentration is dominant is shown in **e**. Scale bars denote 10 μm in all panels. Figure 2.7a is reproduced from Shin et al. (2004) with permission from Proc Natl Acad Sci USA and the remaining images are reproduced from Schmoller et al. (2008) with permission from the American Physical Society

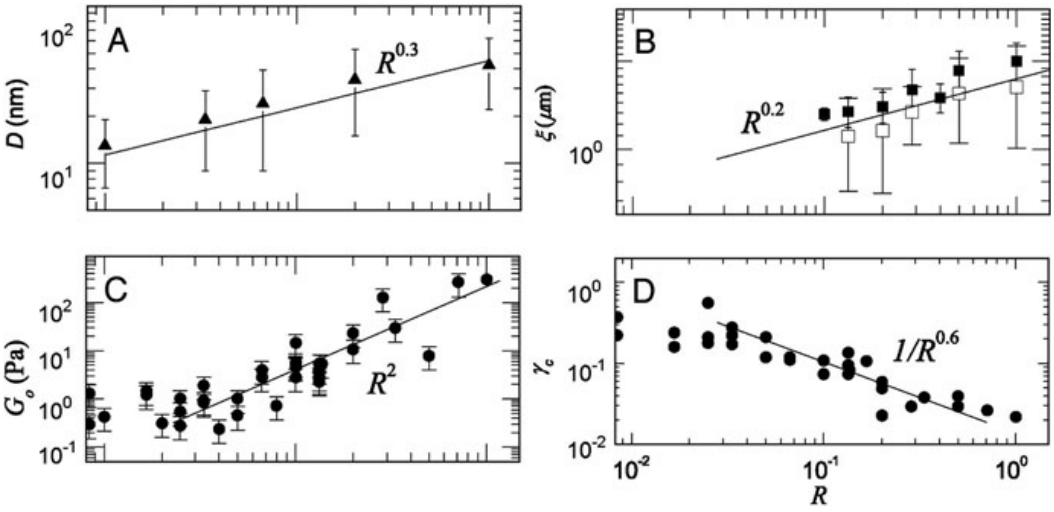

Fig. 2.8 ACLP concentration-dependence of bundle size and mechanical properties of actin networks crosslinked by scruin. Panels **a** and **b** show the increasing of bundle size and mesh size as a linear function of R ([scruin]/[actin]). The corresponding microstructures are shown in Fig. 2.7. Elastic modulus (panel **c**) and critical strain (panel **d**) increases and decreases respectively with increasing R. The scale of R in all panels is the same as shown in panel D. Reproduced from Shin et al. (2004) with permission from the Proc Natl Acad Sci USA

For isotropic meshworks where $\xi \approx l_e$, the storage modulus shows a slightly different dependency on actin concentration such that $G' \sim \kappa_b^2 (ac_A)^{5/2} / (k_B T)$ (MacKintosh et al., 1995). DdFLN (Wagner et al., 2006) and α-actinin (Tseng and Wirtz, 2001) display $G' \sim \varsigma^{0.4}$ and $G' \sim \varsigma^{1.7}$, respectively, when ς

is beyond a certain threshold. Heavy meromyosin (HMM) crosslinked F-actin exhibits $G' \sim \varsigma^{1.2}$ (Tharmann et al., 2007). Therefore, G' depends significantly on the crosslinker density, which determines the mesh size. Similar to pure F-actin networks, actin networks crosslinked by filamin A, DdFLN, and their mutants display a weak frequency dependency of G' and G'' in the low frequency regime (Gardel et al., 2006; Wagner et al., 2006) while filamin A-linked F-actin meshworks have $G'(\omega) \sim G''(\omega) \sim \omega^{0.17}$ in the high frequency regime (Shin et al., 2004). Furthermore, the rupture force of hinged filamins is 10-fold higher than that of non-hinged filamins (Gardel et al., 2006), suggesting that the linkages between domains of ACLPs contribute to the strength of the actin cytoskeleton.

The whole F-actin network shows a decline of G', i.e. a catastrophe, when the imposed strain exceeds a critical value γ^*. One interpretation of the mechanical failure of a crosslinked network is the unbinding of the ACLPs from actin filaments. Thus, the interaction strength between ACLPs and actin may determine the mechanical strength of the whole network. It was found that $\gamma^* \sim \varsigma^{-0.6}$ for scruin-bundled networks as shown in Fig. 2.8 (Shin et al., 2004). In fascin bundled networks, a similar behavior was also observed (Lieleg et al., 2007), and the loading rate-dependence of the rupture force of a single bond was observed for the maximum stress of the whole network even though not all fascin-actin bonds were broken at the same time (Lieleg and Bausch, 2007). The maximum stress of HMM crosslinked F-actin also agrees well with the unbinding force of rigor HMM-actin, and it shows no stress-rate dependencies, which is also consistent with the single bond behaviors (Lieleg et al., 2008). However, curved bundles crosslinked by filamin show no dependence of γ^* on ς (Schmoller et al., 2008), and rupture stress is linearly proportional to c_A and independent of ς (Gardel et al., 2004b). In the nonlinear regime, the differential shear modulus $K'(\sigma) = d\sigma \big/ d\gamma$ may also be used to characterize the actin network sensitivity to stress or strain. $K'(\sigma)$ is a function of crosslinking density but independent of c_A when the stress is over a certain threshold, and $K'(\sigma) \sim \sigma^{3/2}$ for scruin bundled F-actin (Gardel et al., 2004a). However, fascin-bundled F-actin exhibits $K' \sim \varsigma^{3/2}$ (Lieleg et al., 2007). Another possible reason for stress softening is the buckling of actin filaments, though it would primarily occur at very high stresses (Chaudhuri et al., 2007).

The actin cytoskeleton of intact cells has multiple ACLPs, and F-actin filaments are crosslinked into both bundles and branched networks. Competitive binding and cooperative binding between ACLPs potentially exists. In some developmental systems, two or more ACLPs are needed to work in concert to build necessary cellular structural elements. In terms of cellular mechanics, different crosslinkers also show a diverse array of interactions, ranging from additive to non-additive effects (Girard et al., 2004; Reichl et al., 2008). However, there is limited experimental data on the cross-talk between ACLPs in purified systems. Conceptually, synergistic enhancement of mechanical properties can be theoretically generated just by the welding of two structurally complementary sub-networks crosslinked by two different types of ACLPs. Two examples illustrate the diversity of possibilities. First, fascin and filamin crosslinked actin network displays both bundled and branched

microstructures; yet these networks display little cross-talk between the two proteins since the corresponding mechanical properties appear to be determined by the dominant ACLP as shown in Fig. 2.7 (Schmoller et al., 2008). By contrast, actin networks crosslinked by α-actinin and fascin displayed synergistic enhancement of elasticity (Tseng et al., 2005). The underlying mechanism may be the complement between bundled and orthogonal branched networks. Actin networks crosslinked by α-actinin and filamin exhibit more solid-like behaviors than those crosslinked by the individual crosslinkers, specifically displaying increased $G'(\gamma)$ at low γ regime with little enhancement of $G'(\omega)$ as shown in Fig. 2.9 (Esue et al., 2009). Thus, further experiments are needed to fully elucidate the crosstalk between other ACLPs and their synergistic effects on the mechanical properties of purified actin networks.

Crosslinked networks can also be described as affine or nonaffine. In general, in the high strain regime, the deformation of the whole network remains affine and microscopically every filament has almost the same strain, whereas in the low strain regime the deformation may be nonaffine. The transition from nonaffine to affine is controlled by three length parameters: filament contour length L_c, distance between crosslinkers l_c(∼mesh size ξ) and material length l_b that is defined as $l_b = \sqrt{\kappa_b/\mu}$, where μ is the stretch modulus of the filaments (Wilhelm and Frey, 2003; Head et al., 2003; Das et al., 2007; Buxton and Clarke, 2007). The transition can be measured by $\lambda = L_c/\sqrt[3]{l_c^3/l_b}$. Independent of the strain magnitude, nonaffine deformation and affine deformation occur when $\lambda < 2$ and $\lambda > 20$, respectively, and transient behaviors exist in the range of $2 < \lambda < 20$. For a fixed contour length (actin dynamics reaches steady state), elasticity is dominated by the stretch modulus under high crosslinker density or small l_c conditions (affine); the bending modulus dominates under low crosslinker density or large l_c conditions (nonaffine). The apparent strain-stiffening during deformation is basically a nonaffine to affine transition (Onck et al., 2005; Gardel et al., 2004b). The nonaffine-affine transition theory also successfully

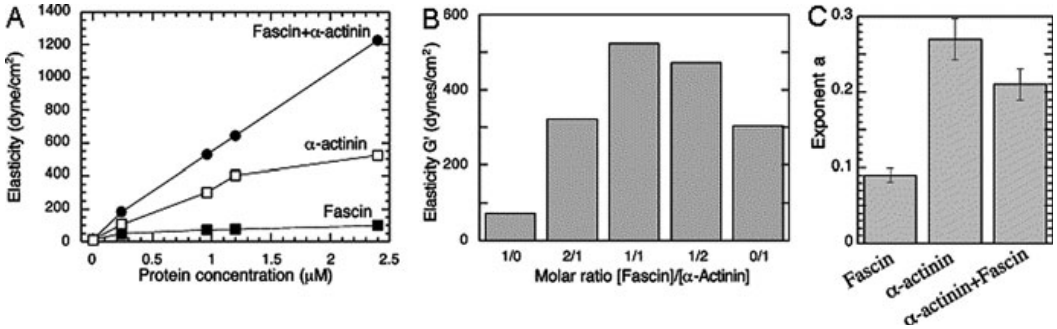

Fig. 2.9 Mechanical properties of actin networks crosslinked by α-actinin and fascin. The synergistic effect on the elasticity of α-actinin and fascin is shown in **a**. The elasticity displays [fascin]/[α-actinin] dependence in **b**. The exponent of the elasticity as a function of frequency is shown in **c**. The total concentration of ACLPs is 0.96 μM in **b** and **c** and the actin concentration is 24 μM for all panels. Reproduced from Tseng et al. (2005) with permission of Elsevier

interprets the scalings between G'(or K') and c_A, ς and the pre-stress observed in these experimental systems. The corresponding microstructural transition was observed in scruin-bundled actin network by confocal microscopy (Liu et al., 2007).

2.2.2.3 Effects of Myosin II on the Mechanical Properties of the Actin Network

In the absence of ACLPs, myosin II motors pull on actin filaments along their axial directions as shown in Fig. 2.10b. Over time, actin filaments aggregate, resulting in a heterogeneous distribution of actin filaments (super-precipitation). In the presence of saturating ATP, active myosin II does not change the shear modulus of an actin filament solution, whereas in the absence of ATP, inactive myosin II crosslinked F-actin, leading to a >10-fold enhancement of the shear modulus (Humphrey et al., 2002). Additionally, the decreasing of G'/G'' and the relaxation time associated with active myosin II indicates that myosin II increases the fluidity of the actin network. This apparent fluidization likely arises from cycles of pulling and releasing, which generate local fluctuations inside the actin network.

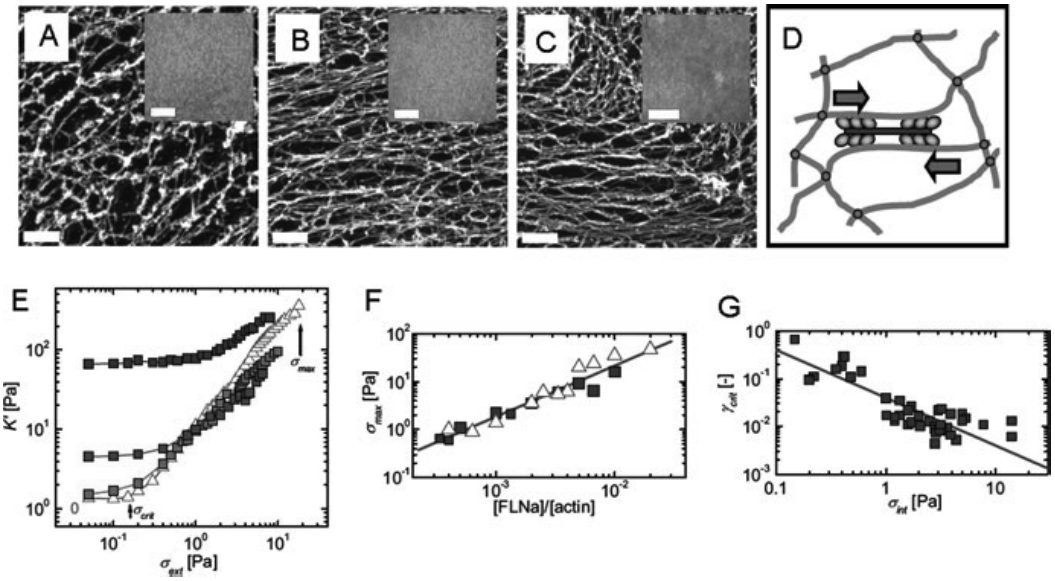

Fig. 2.10 Microstructures and mechanical properties of actin meshwork with muscle myosin II and human filamin A. Electron micrographs of pure actin, actin+myosin ([myosin]/[actin] = 0.02 and 5 mM ATP) and filamin A +myosin+actin ([filamin]/[actin] = 0.005, [myosin]/[actin] = 0.02 and 5 mM ATP) are shown in **a**, **b** and **c**, respectively. The corresponding fluorescent images are found in the inserts. The illustration of an active stiffening mechanism is shown in **d**. Stiffening behaviors of active networks (with myosin to actin ratio of 0.02 (*blue squares*), 0.005 (*green squares*), and 0.001 (*red squares*)) and a passive network at fixed [filamin]/[actin] of 0.005 (*white triangles*) are shown in **e**. The filamin concentration dependence of rupture force is shown in **f**. Critical strain decreases as a function of the internal stress generated by myosin II. Scale bars are 10 μm in all panels. Reproduced from Koenderink et al. (2009) with permission by Proc Natl Acad Sci USA

In the presence of ACLPs, internal tensile stresses associated with the myosin II motor stiffen the actin network, leading to stress-stiffening such that $G'(\omega) \sim G''(\omega) \sim \omega^{1/2}$ (Mizuno et al., 2007). In assembled networks, myosin II and filamin A work together to enhance the network stiffness as shown in Fig. 2.10 (Koenderink et al., 2009). Increasing the myosin concentration leads to higher differential modulus and increasing the filamin A concentration makes the network able to sustain higher stresses. The critical strain displays a power-law decay of the internal stress that is dependent on the myosin II concentration. Because ACLP binding to actin is dynamic, myosin may break the binding between ACLPs and actin when the myosin concentrations become high enough, resulting in the power-law decay of the critical strain with increasing myosin concentration.

2.2.3 In Vivo Measurements of Cell Mechanics

In comparison to reconstituted actin cytoskeletons, the shear moduli of intact cells are several orders higher (Hoffman et al., 2006; Girard et al., 2004; Reichl et al., 2008). One reason for this difference is that there are tens of ACLPs with concentrations on the order of 1 μM in intact cells compared to just one or two ACLPs as in the in vitro experiments. Another reason is that myosin II motors generate contractile forces that not only stiffen the actin network but also enhance the binding between some ACLPs and actin filaments that further increases the stiffness of the actin cytoskeleton (Reichl et al., 2008). In *Dictyostelium*, *myosin II* null cells have decreased cortical tension and elastic moduli compared to wild type cells. Similarly, mutant cells depleted with various ACLPs also have softer cortices as shown in Fig. 2.11 (Girard et al., 2004; Reichl et al., 2008). In the *myosin II* null background, a complex relationship between the ACLPs and myosin II is observed. Some ACLPs (for example, dynacortin) have large effects upon their depletion from a wild type background but smaller effects when depleted from a *myoII* mutant background. By contrast, the depletion of fimbrin has an even more complicated effect being both time-scale sensitive and myosin II dependent: fimbrin contributes only to the viscoelastic moduli on fast time-scales in a wild type background, but also impacts the cortical tension of *myoII* null cells. More generally, similar to the reconstituted actin cytoskeletons, the cytoskeleton of intact cells also display $G'(\omega) \sim G''(\omega) \sim \omega^{3/4}$ in the high frequency regime, indicating that the mechanical properties of cells are dominated by the entropic vibrations of actin filaments at these frequencies. However, in the low frequency range, cells exhibit elastic moduli, $G'(\omega) \sim G''(\omega) \sim \omega^{\beta}$, where $0 < \beta < 0.3$ (Hoffman et al., 2006; Deng et al., 2006; Girard et al., 2004; Reichl et al., 2008). The difference in the low frequency regimes between intact cells and artificial actin cytoskeletons has been primarily attributed to the forces generated by motors that push the system out of thermal dynamic equilibrium (Lau et al., 2003), which is consistent with the in vitro observations (Humphrey et al., 2002; Mizuno et al., 2007). Indeed, *myosin II* null cells have a fundamentally different character in the low frequency range that is more consistent with a passive network (Girard et al., 2006).

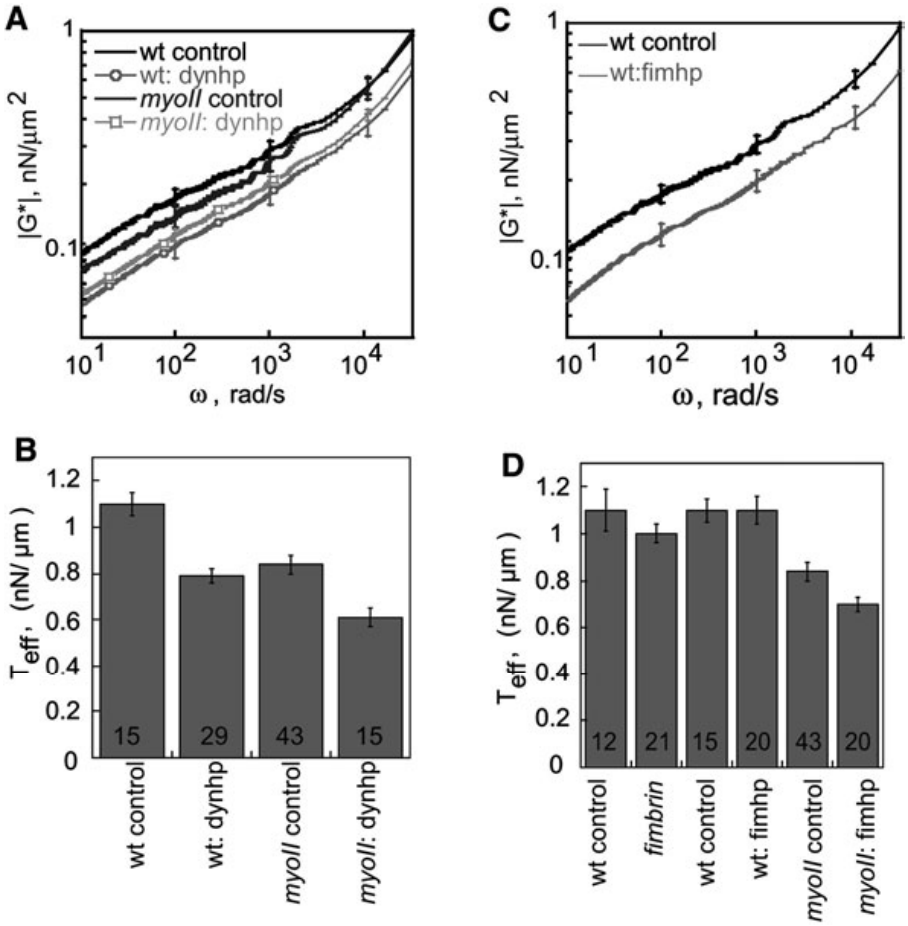

Fig. 2.11 Mechanical properties of *Dictyostelium* cells. **a** and **c** show the frequency dependence of complex moduli of different cell-lines. **b** and **d** show the effective cortical tension for these cells. "wt" and "*myoII*" represent wild-type and *myosin II*-null cells, respectively. "dynhp" and "fimhp" refer to dynacortin-hairpin and fimbrin-hairpin, respectively. Dynacortin and fimbrin are ACLPs, and hairpin constructs are used to silence gene expression through RNA interference. Reproduced from Reichl et al. (2008) with permission of Elsevier

Many of the studies of living cells draw upon laser-based tracking of single or multiple particles embedded in the living network. Because the particles may fluctuate due to thermal or active forces that act on the particles, the fluctuation-dissipation theorem (FDT) is used to extract viscoelastic parameters. However, the FDT should only be applied to systems at equilibrium, not out of equilibrium. Therefore, by measuring the mean square displacement (MSD) of the particles as a function of correlation time, it was found that the FDT cannot describe the particle behaviors in the low frequency regime (Lau et al., 2003; Bursac et al., 2005; Girard et al., 2006; Mizuno et al., 2007; Wilhelm, 2008; Reichl et al., 2008). Furthermore, in some contexts, the FDT is violated because the apparent diffusive behavior has a much larger magnitude than expected, considering the viscous damping for the particle size. This suggests that local active processes can essentially facilitate the stirring of the cytoplasm (Brangwynne et al., 2009). It was further demonstrated that the mechanochemistry of myosin II motors in combination with ACLPs regulates the

MSDs in the low frequency regime (Girard et al., 2006). ACLP mutant cells also display significant effects on the complex modulus over a wide frequency range (Girard et al., 2004). The coupled effect of myosin and ACLPs was also investigated (Girard et al., 2006; Reichl et al., 2008). The frequency-dependent mechanical behaviors of cells imply that microscopic processes, such as unbinding events and conformational changes of ACLPs and motors with a broad distribution of characteristic times play important roles in regulating cell mechanics.

Based on these types of experimental observations, three major cell mechanics models have been proposed: tensegrity (Ingber, 2003), soft glassy rheology (Fabry et al., 2001; Trepat et al., 2007; Zhou et al., 2009) and the sol-gel hypothesis (Janmey et al., 1990). In the tensegrity model, the actin network, including myosin II and ACLPs, is considered to be primary sources of pre-stress (Wang et al., 2001), and cell stiffness is proportional to the pre-stress that cells experience. Tensegrity can help explain the stress-stiffening, but it does not predict the power-law behaviors of cells. The soft glassy rheology (SGR) model considers the cells glassy materials that are microstructurally disordered and thermodynamically close to a glass transition. The deformations in glassy materials are microscopically inelastic, localized and time-dependent. The SGR model successfully accounts for the power-law behavior in the low frequency regime but it does not capture the stress-stiffening. The sol-gel model assumes that the cell is a gel of filamentary polymers embedded within a fluid cytosol, which predicts a weaker frequency dependency in the low frequency regime than is observed experimentally. Thus, all models capture some aspects of cell mechanics, but a single model that accounts for all of cellular behaviors has yet to emerge.

2.3 Functions of the Actin Cytoskeleton in Mechanosensation

Mechanosensing, the sensing of mechanical force, is crucial for a range of processes that extend over a wide range of length- and time-scales and from the molecular to organismal levels. At the cellular level, stretch receptors in the plasma membrane and many components of the cytoskeletal network are obvious targets of external forces. However, internally generated forces are also felt by the same machinery, allowing intrinsic regulation and cross-talk to occur through the heterogeneous cytoskeletal network. Here, we will focus on two mechanisms for mechanosensing in the actin network: the crosslinked actin network complete with myosin II motors, which governs the cell shape changes particularly during cytokinesis (Effler et al., 2006; Ren et al., 2009) and the actin-associated proteins found in focal adhesions (Vogel and Sheetz, 2006).

2.3.1 Mechanosensing Through Myosin II and Actin Crosslinking Proteins

Dividing cells have a mechanosensory system that they use to monitor their shape as they cleave into two daughter cells. The system could be activated in a controlled

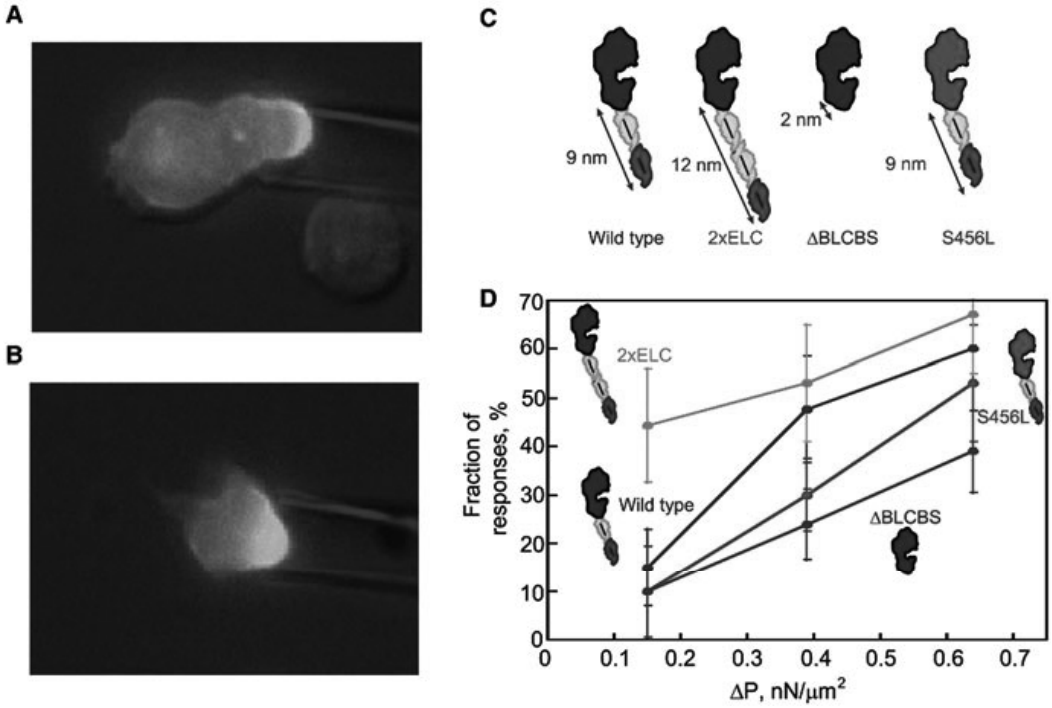

Fig. 2.12 Mechansensing system in *Dictyostelium*. **a** and **b** show the accumulation of fluorescently labeled cortexillin I and myosin II, respectively. Cortexillin I and myosin II are green. The microtubules are labeled red with RFP-tubulin. The lever arm length of different myosin II mutants is shown in **c**. The percentage of cells displaying mechanosensing increases with elevated pressure as shown in **d**. Reproduced from Ren et al. (2009) with permission of Elsevier

fashion, using micropipette aspiration (Effler et al., 2006). Here, myosin II and the actin crosslinker cortexillin I accumulate cooperatively in highly deformed regions in dividing wild type cells as shown in Fig. 2.12. Both myosin-II and cortexillin-I are necessary for this function since cell-lines devoid of either protein are unable to respond to cellular deformations (Ren et al., 2009). Furthermore, only fully wild type myosin-II and wild type cortexillin are able to fully restore mechanosensing while many of the functions of each protein are expendable for cytokinesis contractility (Ren et al., 2009). Except for cortexillin-I, other ACLPs that play a major role in cytokinesis and the microtubules may be dispensed for mechanosensing in dividing *Dictyostelium* cells (Effler et al., 2006). In sum, these observations indicate that the cooperative interaction between myosin II and cortexillin I provide the core of the mechanosensor.

Myosin-II mechanochemistry appears to be the essential active component of the mechanosensory module. Regulatory light chain phosphorylation leads to the activation of *Dictyostelium* myosin-II. Interestingly, this phosphorylation step is essential for mechanosensing (Ren et al., 2009) but is not required for cytokinesis (Beach and Egelhoff, 2009). The lack of a requirement for light chain phosphorylation in cytokinesis is likely due to the fact that RLC phosphorylation only leads to a 3-5-fold activation of the actin-activated ATPase activity in *Dictyostelium* myosin II, and that the myosin II mechanochemistry is not rate limiting for cytokinesis over at least a 30-fold range (Zhang and Robinson, 2005; Chen et al., 1995). By contrast, many

other myosin II isoforms are activated ~30-fold by RLC phosphorylation. However, with respect to mechanosensing, this observation suggested that the motor domain of myosin-II was the critical active component of cellular-scale mechanosensing. To test this, the maximum force (F_{max}) of the myosin-II was shifted by altering the lever arm length ($F_{max} \propto$ lever arm length^{-1}), which shifted the applied pressure-dependency of the mechanosensory response (Uyeda et al., 1996; Ren et al., 2009). Because myosin-II must undergo a full lever arm swing before it can release its ADP, this result strongly indicates that the local accumulation of myosin-II is regulated by the kinetics of its binding/unbinding to actin filaments. It is also likely that the extent of accumulation during mechanosensing is proportional to the magnitude of the applied force as shown in Fig. 2.12 (Ren et al., 2009), which is consistent with catch-bond behaviors of myosin II (Guo and Guilford, 2006).

The regulated assembly and disassembly of myosin II into bipolar thick filaments (BTFs) is also required for the mechanosensory system. Without assembling into BTFs, myosin II cannot generate contractile force and therefore experience tension. Because myosin II accumulates during the mechanosensory response, unassembled monomeric myosin II must be able to diffuse to the site, requiring these myosins to be disassembled. Therefore, the full assembly/disassembly dynamic is required for this process. It should be noted that myosin-II BTF assembly in *Dictyostelium* is independent of myosin-II light chain phosphorylation but is fully dependent on the heavy chain phosphorylation. In contrast, mammalian myosin II assembly is regulated by both heavy chain and regulatory light chain phosphorylation (Beach and Egelhoff, 2009 and references therein). Regulatory light chain phosphorylation results in a conformational change from a thick filament assembly incompetent state to an assembly competent state (the so-called 10S – 6S transition) (Craig et al., 1983). Because *Dictyostelium* myosin-II does not undergo this transition, it does not require the RhoA-ROCK kinases pathway for regulation of contractility. Consistently, the *Dictyostelium* genome is devoid of ROCK kinase.

Dividing cells have distinctive mechanical properties (the cells soften from anaphase through cytokinesis completion) and the global/polar actin crosslinkers (dynacortin, fimbrin, and enlazin) become more cytoplasmic as compared to interphase cells (Robinson and Spudich, 2000; Reichl et al., 2008). Similarly, wild type cells show a much stronger mechanosensory response during cell division than during interphase. However, the mechanosensitive localization occurs very strongly in interphase *RacE* null cells (Ren et al., 2009). Unlike RhoA that regulates myosin-II functions, RacE, a Rac-family small GTPase, is known to be upstream of global ACLPs, such as dynacortin, enlazin and fimbrin (Robinson and Spudich, 2000; Zhang and Robinson, 2005). Experimental data shows that the cortical stiffness of *RacE* null cells is much lower (70% lower) than that of wild type cells, indicating RacE helps to maintain the mechanical integrity of the actin cortex. It is not known yet whether RacE directly inhibits the mechanosensory pathway or if the mechanosensory response only occurs within a certain range of cortical stiffness.

The molecular mechanisms for the cooperative accumulation of myosin II and cortexillin I remain to be fully defined. However, there are four processes that may contribute to their accumulation. The first is that forces stabilize the bipolar

thick filaments in highly deformed region by increasing the binding life time of myosin-actin. This tight binding then promotes additional myosin accumulation through cooperative interactions between motor domains of assembled (in BTF form) and unassembled myosin monomers. The second mechanism is that the binding of cortexillin and the binding of myosin to actin filaments facilitate each other, i.e. cortexillin and myosin II may bind actin cooperatively. A third possible mechanism is that the curvature sensitivity of phosphatidylinositol 4,5-diphosphate (PIP_2) lipid molecules might lead to PIP_2 accumulation in the pipette, resulting in cortexillin accumulation since cortexillin binds PIP_2 (Stock et al., 1999). Consequently, the cortexillin accumulation increases the local stiffness of the actin network and enhances the force propagation, which can potentially lead to myosin II accumulation through the first mechanism. Finally, the fourth possible mechanism is that BTF assembly regulatory enzymes, including MHCK and myosin heavy chain phosphatase (which is less well characterized), may be force sensitive. The reduced phosphorylation (by inhibiting MHCK or activating the myosin heavy chain phosphatase) of myosin heavy chains with increasing force could promote local accumulation of the BTFs. However, force-sensitive activation or inhibition of these enzymes may not be essential; rather the enzymes may only be required to maintain the available free pool of myosin monomers, which is essential for the mechanosensory response. These four mechanisms are not mutually exclusive. In the next sections, we will show how force-dependent promotion of BTF assembly and cooperativity between myosin II and cortexillin might lead to the inter-dependent, mechanical stress-induced accumulation of these proteins.

2.3.1.1 How Force Might Modulate Myosin II Bipolar Thick Filament Assembly

To consider where force might act in myosin BTF assembly, a sensitivity analysis of the BTF assembly pathway was assessed. The reactions of myosin II assembly and the corresponding reaction rates are listed in Table 2.1. M_0, M, D and T represent phosphorylated (assembly incompetent) monomer, unphosphorylated (assembly competent) monomer, dimer and tetramer, respectively. BTF_3, BTF_n and

Table 2.1 Kinetics of myosin II assembly based on the dimer addition model. Reproduced from Ren et al. (2009) with permission of Elsevier

$M_0 \underset{k_{-1}}{\overset{k_1}{\rightleftharpoons}} M,$	$k_1 = 0.0008\ \mathrm{s}^{-1}$ $k_{-1} = 0.1\ \mathrm{s}^{-1}$
$M + M \underset{k_{-2}}{\overset{k_2}{\rightleftharpoons}} D,$	$k_2 = 0.37\,\mu\mathrm{M}^{-1}\mathrm{s}^{-1}$ $k_{-2} = 0.01\ \mathrm{s}^{-1}$
$D + D \underset{k_{-3}}{\overset{k_3}{\rightleftharpoons}} T,$	$k_3 = 0.0395\,\mu\mathrm{M}^{-1}\mathrm{s}^{-1}$ $k_{-3} = 0.0045\ \mathrm{s}^{-1}$
$T + D \underset{k_{-4}}{\overset{k_4}{\rightleftharpoons}} \mathrm{BTF}_3,$	$k_4 = 1.25\,\mu\mathrm{M}^{-1}\mathrm{s}^{-1}$ $k_{-4} = 0.025\ \mathrm{s}^{-1}$
$\mathrm{BTF}_n + D \underset{k_{-5}}{\overset{k_5}{\rightleftharpoons}} \mathrm{BTF}_{n+1},$	$k_5 = 10\,\mu\mathrm{M}^{-1}\mathrm{s}^{-1}$ $k_{-5} = 0.2\ \mathrm{s}^{-1}$

BTF_{n+1} are the bipolar filaments having 6, $2n$ and $2(n+1)$ monomers, respectively. The formation of the anti-parallel tetramer T is the nucleation step, and the subsequent steps are the growth phase of BTF assembly where dimers D are added to the BTF. The reaction rates are derived from a combination of in vitro kinetic studies of BTF assembly as well as in vivo fluorescence recovery after photobleaching experiments (Mahajan and Pardee, 1996; Moores and Spudich, 1998; Reichl et al., 2008; Ren et al., 2009). From this analysis, the most likely process that may be affected is the ratio of k_1 to k_{-1}. Figure 2.13 shows the kinetics of assembly after this ratio is shifted ten-fold, which could mimic inhibition of MHCK, activation of myosin phosphatase, or a lowering of the energy barrier required for incorporating M_0 into

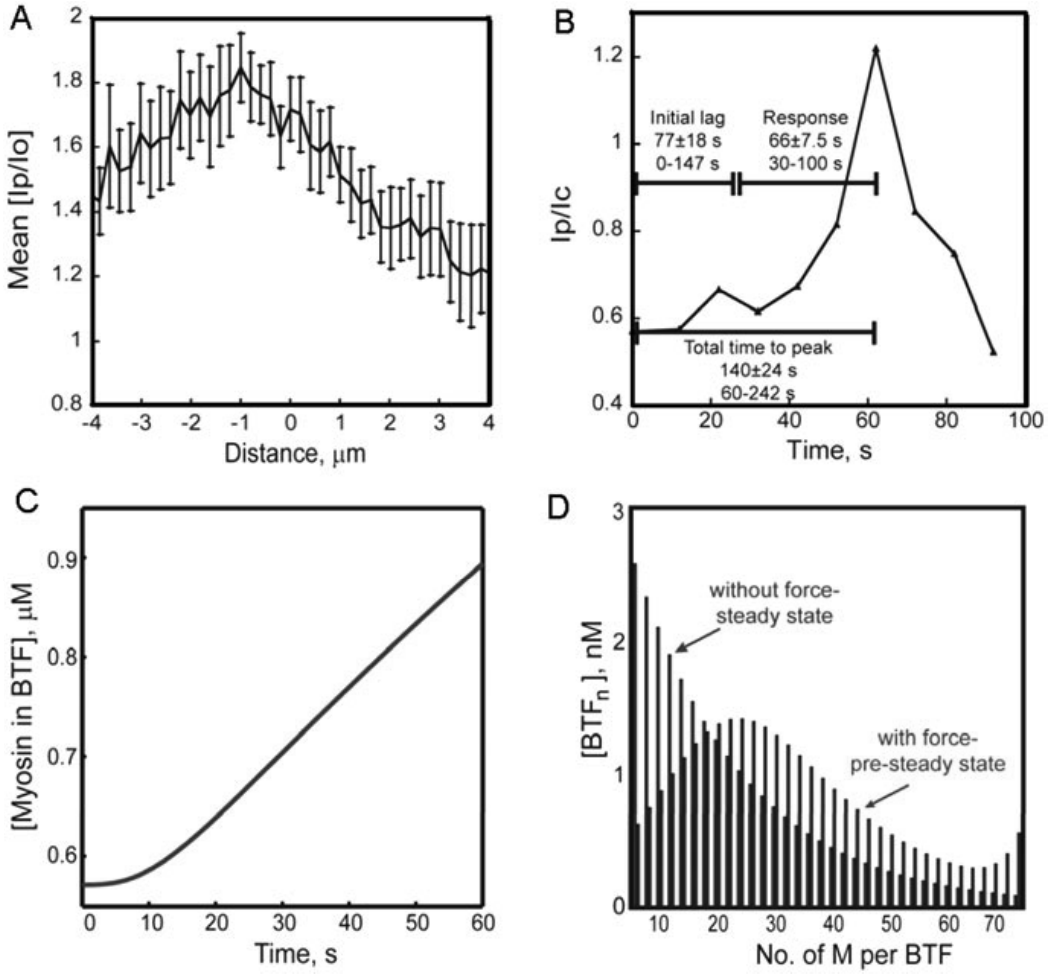

Fig. 2.13 Accumulation of myosin II in response to force in *Dictyostelium* cells during anaphase: (**a**) spatial distribution of myosin II intensity in pipette region normalized by the intensity at the opposite pole of the cell; (**b**) averaged transient curve of myosin II accumulation where intensity is normalized by the intensity in the cytoplasm; (**c**) simulation result of the kinetics of myosin II accumulation when k_{-1} in Table 2.1 is decreased by 10 fold to mimic the force effect; (**d**) the BTFs distribution before (without force) and 60 s after 10-fold change in k_{-1}. Reproduced from Ren et al. (2009) with permission from Elsevier

a pre-existing BTF. The force dependence of these steps generally can have the form similar to Eq. (2.1).

Overall, this analysis suggests that the largest impact on the assembly mechanism might be in the transition from assembly-incompetent to assembly-competent states. Although force might act on MHCK or a myosin heavy chain phosphatase, this scenario requires additional enzymes and steps. A very appealing mechanism is one where motor domains found in pre-existing mini-BTFs are stabilized in the mechanical transition state by force, which then leads to the local accumulation of myosin monomers, putting them in close proximity to the BTF where they can be directly inserted. The motors found in the HMM form of myosin II (dimeric but unassembled myosin monomers; see Fig. 2.2) binds actin in a highly cooperative fashion but only during the transition state of the actomyosin-ADP+P_i complex (Tokuraku et al., 2009) or if the actin structure has been altered such as by being assembled with Ca^{2+}cations (Ca^{2+}•ATP-actin – as opposed to Mg^{2+}•ATP-actin found in cells) (Orlova and Egelman, 1997). This mechanism has the appeal that no additional enzymes are required, and that all of the necessary parts are included directly in the myosin motor and thick filament assembly region. In this model, the MHCK and myosin heavy chain phosphatase are still required to maintain the pool of available myosin monomers M_0 and to ensure that the system relaxes back once the mechanical signal subsides. However, more experiments are required to see if this mechanism accounts for mechanosensitive BTF assembly.

2.3.1.2 Cooperativity Between Myosin II and Cortexillin

Since myosin II-binding to actin can be highly cooperative depending on the actin conformation and the transition state of the motor-actin complex (as discussed in the previous section), it is very tempting to consider that this cooperativity may be extended to interactions between myosin and actin-associated proteins. For muscle myosin II, the motors bind cooperatively to actin filaments, but only in the presence of tropomyosin-troponin (Geeves and Halsall, 1987; Hill et al., 1980; Chen et al., 2001). On the other hand, the binding of actin-binding proteins (ABPs), such as scruin (Owen and DeRosier, 1994) and formins, induces noticeable structural changes in F-actin. Since F-actin is the common binding substrate of myosin II and ACLPs, it is possible that the binding of myosin and ACLPs to actin are cooperative, i.e. the structural changes in F-actin due to one kind of binding facilitate another kind of binding (Williamson, 2008). Mathematically, the cooperativity between myosin II and cortexillin can be written as

$$\frac{dC_{\mathrm{M}}}{dt} = g\left(C_{\mathrm{C}}\right) - \left(k_{\mathrm{on}}^{\mathrm{M}} C_{\mathrm{M}} - k_{\mathrm{off}}^{\mathrm{M}}\right) \text{and} \frac{dC_{\mathrm{C}}}{dt} = h\left(C_{\mathrm{M}}\right) - \left(k_{\mathrm{on}}^{\mathrm{C}} C_{\mathrm{C}} - k_{\mathrm{off}}^{\mathrm{C}}\right). \quad (2.11)$$

where C is the concentration. The superscripts/subscripts M and C represent myosin and cortexillin, respectively. g and h are functions characterizing the cooperativity between the two proteins. Here, only positive cooperativity is considered and

both g and h always have non-negative values. Furthermore, because of the force-dependence of myosin-actin binding, $k_{\text{off}}^{\text{M}}$ is assumed to be a function of force, i.e. $k_{\text{off}}^{\text{M}}(f) = k_{\text{off}}^{0} \exp\left(\frac{f\Delta x}{k_{\text{B}}T}\right)$.

2.3.2 Mechanosensation Through Focal Adhesion Complexes

Mechanosensitive behaviors of focal adhesions (FAs) are important in many cellular processes such has cell growth, differentiation and motility. FAs are mechanical linkages between the cytoskeleton and the extracellular matrix (ECM). FAs are large multi-molecular complexes that can extend several-micrometers and consist of a large number of different proteins, including integrins and ABPs such as talin, vinculin, paxillin, and tensin (Zamir and Geiger, 2001; Geiger et al., 2009). In FAs, integrins form heterodimers consisting of α and β subunits non-covalently bound and each consisting of an extracellular domain, a single-pass transmembrane helix, and a short cytoplasmic tail (Puklin-Faucher and Sheetz, 2009). The tail of β-integrin binds to the talin head domain. Talin may then anchor directly to actin or indirectly through vinculin. FAs can be stationary or mobile while displaying a continuous exchange of components with the cytoplasmic pool. FAs grow with increasing local force (Tan et al., 2003) and tend to orient in the direction of applied force (Riveline et al., 2001), which has been attributed to stretching forces, which may enhance the binding affinity of integrins to the ECM (Katsumi et al., 2005).

FA formation is initiated with the activation of integrins. Inactive integrins adopt a bent shape whereas the active forms have an extended shape (Hynes, 2002 and references therein). Integrins may be activated either by their head binding to the ECM (so-called outside-in signaling) or by the tail binding to talin (so-called inside-out signaling). The activation of the head and the resulting binding to the ECM are thought to occur through long-range conformational changes that propagate through the integrin extracellular domain. Activation of integrin $\alpha_5\beta_1$ in cells can be switched on mechanically, and the corresponding strength of FAs increases with the rigidity of the extracellular matrix, indicating that the integrin-ECM interaction fits a catch-bond model (Friedland et al., 2009). Single molecule measurements have also shown that the catch-bond behavior of integrin $\alpha_5\beta_1$ may be attributed to the mechanical activation of the headpiece, but not integrin extension, over a force range of 4–30 pN (Kong et al., 2009).

The next mechanosensitive protein in the FA is talin, a large protein consisting of an N-terminal head region and a long rod region. Near talin's amino-terminus is a FERM (band 4.1, ezrin, radixin, moesin) domain through which talin binds to integrin, focal adhesion kinases (FAKs) and other receptors. Talin-binding to the integrin β tail disrupts an intracellular salt bridge between the α- and β-integrin subunits, increasing the integrin affinity for ECM (Tadokoro et al., 2003). Additionally, talin has eleven vinculin binding sites (VBSs) in its rod region. Single molecule measurements discovered that only one VBS is active in the absence of force and

two more VBSs appear when the talin rod is stretched by relatively low (12 pN) forces (del Rio et al., 2009). In the absence of force, these two force-sensitive VBSs are thought to remain buried in adjacent amphipathic helices through hydrophobic interactions.

Talin then links to vinculin, a 116 kDa actin-binding protein, which links the core FA proteins to the actin cytoskeleton. The vinculin head domain consists of seven α-helices arranged as two four-helical bundles (eight α-helices), and its tail domain has five α-helices that form an anti-parallel bundle. The strong interaction between the head and the tail masks the binding sites for other proteins such as talin, F-actin, α-actinin and paxillin and keeps vinculin in its inactive states. Upon talin-binding to α-actinin, the tail domain of vinculin is displaced away from the head domain, which activates vinculin (Izard et al., 2004) and enables its binding to F-actin and other molecules.

The mechanical stretching of FAs triggers many downstream signaling pathways by activating the SH2 domain-containing phosphatase SHP-2 and non-receptor protein tyrosine kinases, such as Src and FAK (Tamada et al., 2004; Giannone and Sheetz, 2006). These enzymes regulate the assembly/disassembly of FAs by controlling the actin stress fiber (actin bundles with myosin II thick filaments) formation (Vicente-Manzanares et al., 2009). Activity of some of these kinases, such as FAK kinase, requires actin and myosin II-dependent tension (Tilghman and Parsons, 2008). Furthermore, stretching of p120Cas in cells or using an in vitro reconstitution system exposes more Src kinase binding sites and leads to its local activation (Sawada et al., 2006). This stretch-induced activation can be very fast as Src at remote sites may be activated within 0.3 s, demonstrating just how fast signals can propagate through the elastic cytoskeleton (Na et al., 2008).

2.3.3 The Actin Cytoskeleton Works as a Force-Transmission Highway

Both chemical and mechanical signals can be transmitted over long distances. Propagation of chemical signals occurs mainly through the diffusion of molecules in the cytosol and its speed is limited by the chemical reaction (such as phosphorylation) rates, unbinding/binding rates and diffusion rates. Diffusion is usually the limiting step since the diffusion coefficient of molecules in cells is in the range of 0.01–100 $\mu m^2 s^{-1}$, depending on the molecular size and shape and the viscosity of cytoplasm on the length-scale of the diffusing particle (Howard, 2001). For example, it can take one molecule 1–100 s to travel 10-μm using diffusion alone. On the other hand, mechanical signals may be transmitted through the deformation of cytoskeleton along actin filaments, microtubules and intermediate filaments. The speed of transmission depends on the elastic modulus of the cytoskeleton where signals may propagate over a 10-μm distance on sub-second time-scales, indicating that proteins in cells can sense mechanical stimuli much more rapidly than chemical signals (Forgacs, 1995). This propagation of mechanical deformations likely

depends on the pre-stress as well as the elastic modulus of the cytoskeleton, and the magnitude of deformation decays exponentially in space with a characteristic length that is comparable to or larger than the size of the cell (Wang and Suo, 2005).

One consequence of signal propagation through the integrated elastic actin cytoskeleton is that signals can be transmitted over long distances and broad areas and to a range of organelles. For example, actin filaments are connected to the nuclear envelope through a complex of SUN and nesprin proteins (Wang et al., 2009), to the plasma membrane through proteins such as ezrin, radixin, and moesin (ERM proteins) (Sato et al., 1992), to stretch-activated channels (SACs) by myosin I motor proteins (Fettiplace and Hackney, 2006), and to mitochondria by mitochondrial ABPs (Boldogh et al., 1998). Forces transmitted by the actin cytoskeleton to the nucleus alter gene expression, which may in turn regulate actin remodeling. The SACs can also be activated or deactivated by cytoskeleton stretching, resulting in ion flux, regulating stress fiber formation and orientation and myosin II bipolar thick filament assembly. Mechanical stimuli propagated to membrane-bound or associated proteins through the actin-membrane connections can lead to changes in activity of membrane-bound signaling molecules and other ion channels.

2.4 Remodeling of the Actin Cytoskeleton During Mechanosensation

The actin cytoskeleton is composed of highly dynamic structures. Besides mechanosensing and transmitting mechanical signals, the cytoskeleton can rearrange its structures in response to the mechanical stimuli – this is referred to as remodeling. Actin remodeling is determined by ABPs that control linear elongation, shortening and organization of actin filaments in response to signaling cascades (Stossel et al., 2006). However, superimposed over these mechanosensitive actin-binding proteins are signaling molecules, such as kinases, Rho-family GTPases (e.g. RhoA, Cdc42 and Rac), phosphoinositides and WASP-family proteins, which are also spatially and temporally coordinated biochemically and, indirectly, mechanically.

Most Rho proteins switch between active (GTP-bound) and inactive (GDP-bound) conformations. The activities of Rho proteins are regulated by Rho guanine nucleotide exchange factors (Rho-GEFs) and Rho GTPase-activating proteins (Rho-GAPs). The Rho-GEF promotes the exchange of GDP for GTP while the Rho-GAPs enhance GTP hydrolysis. Rho guanine-nucleotide dissociation inhibitors (GDIs) also bind to prenylated GDP-bound Rho proteins and allow their translocation between membrane and the cytosol (Buchsbaum, 2007). RhoA and its effector Rho-kinase elevate myosin II light chain phosphorylation and thereby promote myosin II activation. Cdc42 activates WASP, which subsequently mediates the branched actin-network formation by activating Arp2/3 (Pollard, 2007). PIP_2 can induce G-actin dissociation from actin-monomer-binding proteins and

uncapping of the actin filament barbed ends, and can enhance the linkages between the actin cytoskeleton and the plasma membrane by activating ERM proteins (Nebl et al., 2000). PIP_2 can also activate vinculin, promoting FA assembly (Sechi and Wehland, 2000), and WASP, increasing actin polymerization (Pollard, 2007).

2.4.1 How Mechanically Activated Kinases Regulate the Actin Cytoskeleton

Mechanically induced FAs trigger the activation and recruitment of many downstream kinases (Brakebusch and Fässler, 2003), and these kinases affect actin remodeling by regulating small GTPases and ABPs. Focal adhesion kinase binds to integrin, talin and paxillin, and this binding enhances FAK activities, which promotes stress fiber formation by increasing the recruitment of talin and paxillin. Integrin-linked kinase (ILK) binds the tails of β integrin subunits, paxillin and phospholipids, which induces the phosphorylation of PKB/AKT protein kinases that are upstream of actin polymerization. ILK also forms a complex with other proteins to recruit F-actin to FAs. The FAK-Src complex stimulates Rac1 activity, recruits the GEF for Cdc42 and Rac1, and mediates the suppression of Rho-GTP by regulating Rho-GEFs and Rho-GAPs (Huveneers and Danen, 2009 and references therein).

2.4.2 Crosstalk Between Microtubules and Actin Cytoskeleton

Increasing evidence shows crosstalk between microtubules and actin cytoskeleton. For example, centrosome separation and positioning during mitosis depend on the integrity of the actin cytoskeleton and F-actin cortical flow (Rosenblatt et al., 2004). By contrast, actin nucleation near the plasma membrane is coordinated by microtubules and microtubule-associated proteins (Martin et al., 2005; Siegrist and Doe, 2007; Rosales-Nieves et al., 2006). Similar to the concept of the tensegrity model, cortical motors may pull on astral microtubules and conversely, astral microtubule polymerization exerts a pushing force against the actin cortex, promoting centrosome separation and positioning. The activation of Src was observed at cortical sites where microtubules appear to deform the cortex (Na et al., 2008). Microtubules also affect the spatial distribution of active small GTPases, thereby regulating the organization of the actin cortex (Siegrist and Doe, 2007 and references therein), and many unproven mechanisms have been proposed for this crosstalk. However, the list of structural linkages between microtubules and F-actin continues to grow. Among the first identified linkages was the splice-variant of the mitotic kinesin-like protein (MKLP1) called CHO1. CHO1 has a kinesin-family motor domain, which can move on microtubules, and an additional microtubule-binding domain and an F-actin binding domain in its tail (Robinson and Spudich, 2004). Indeed, MKLP1 proteins help organize the central spindle microtubules, and CHO1 can integrate this

system with the cortical actin network. In *Drosophila melanogaster*, cappuchino (an FH_2 containing protein) and spire (a WH_2 containing protein) can crosslink microtubules and actin filaments (Rosales-Nieves et al., 2006). In *Schizosaccharomyces pombe*, tea4p and tea1p also localize to the plus ends of microtubules, and a complex of tea1p, tea4p and the formin for3p is necessary for the establishment of cell polarity and actin nucleation at new cell ends (Martin et al., 2005). Thus, several linkages between the actin and microtubule networks promote their integration and may facilitate force-propagation, and therefore signal-propagation, through these systems.

2.5 Experimental Techniques for Measuring Mechanosensation – In Vitro and In Vivo Methods

In addition to traditional micropipette aspiration (MPA), the past few decades have witnessed the development of various new techniques using the combinations of nanomanipulation, microfabrication, magnetic techniques, and optical techniques (Bao and Suresh, 2003; Addae-Mensah and Wikswo, 2008). These methods include atomic force microscopy (AFM), magnetic tweezers, optical tweezers, magnetic twisting cytometry (MTC), particle-tracking microrheology (PTM), microfluidic devices, stretching devices, traction force microscopy (TFM) and MEMS-based devices. Classic MPA still offers a number of advantages in that it is relatively easy to implement and can be readily adapted to a broad array of cell-types, particularly those which are not highly adherent. MPA can be used to measure effective tension and elastic and viscous properties of the cell. Perhaps more significantly, MPA is very useful for imposing deformations to cells so that the cell's response may be monitored using an array of fluorescence methods. However, the major limitation of MPA is that it is difficult to measure properties occurring on fast sub-second timescales or to measure frequency-dependent features. For these sorts of measurements, many of the other methods, for example AFM, MTC and PTM, are more suitable (Girard et al., 2004; Hoffman et al., 2006). PTM can be categorized into single-bead, two-bead and multiple-bead modes (Wirtz, 2009). Depending on the driving force, PTM has two working modes: passive and active. To measure the mechanical properties of single molecules, AFM is commonly used for the high force ranges (>10 pN) whereas optical tweezers and magnetic tweezers are commonly used for relatively low forces (Neuman and Nagy, 2008; Finer et al., 1994). AFM and optical tweezers also allow three-dimensional manipulation of molecules. AFM is often used to study protein folding/unfolding and protein-protein interactions while tweezers are usually used to study biological motors, including cytoskeletal motors and DNA and RNA polymerases. Additionally, many of these methods have been combined with fluorescence microscopy techniques, such as total internal reflection fluorescence (TIRF) imaging and fluorescence resonance energy transfer (FRET) (Sarkar et al., 2004; Moffitt et al., 2008; del Rio et al., 2009).

Microfluidic devices and flow chambers are used to study the cell responses to shear flow (del Álamo et al., 2008; Wang and Levchenko, 2009). Stretching devices

are usually coupled with fluorescence imaging methods to quantify the effects of stretch on actin cytoskeleton rearrangement, activation of kinases, gene expression and cell differentiation (Sawada et al., 2006; Kurpinski et al., 2006). TFM was invented to investigate the traction force that cells apply to the substrates (Pelham and Wang, 1997). Initially, TFM methods utilized fluorescent beads embedded in polymeric substrates so that traction forces exerted by adherent cells on the substrate could be calculated from the displacements of the beads. Recently, micropatterned substrates by soft photolithography have been used to control the cell adhesion areas and cell shapes (Balaban et al., 2001; Tan et al., 2003; Théry and Bornens, 2006). Therefore, a broad range of mechanical measurements and manipulations are now possible across a broad array of length- and time-scales and from the molecule to cellular levels.

2.6 Conclusion and Perspectives

Mechanical inputs must have been among the first signals that cells received and had to respond to, and the ability of cells to sense and react to these inputs likely evolved at a very early time point. Thus, it is not surprising that there are numerous overlaps between the mechanotransduction and "traditional" chemical signal transduction pathways. Because of the overlap between these pathways, mechanical-chemical coupling and feedback loops are a natural consequence of this system integration. Because the actin cytoskeleton is structurally integrated with nearly every aspect of the cell, mechanical inputs can be transmitted quickly throughout the cell. Furthermore, individual proteins may be involved in multiple pathways and contributing multiple functions. Therefore, to fully understand the roles of individual proteins and the cooperativity among them in the actin cytoskeleton, in vitro experiments involving single molecule measurements, reconstituted actin networks, and computational simulations of protein folding/unfolding and protein-protein interactions have to be combined with quantitative in vivo observations. Challenges for understanding mechanosensation through the actin cytoskeleton include revealing how proteins function cooperatively over short nanometer-length-scales and fast sub-second time-scales. Direct observations of force propagation in cells and eventually between cells within tissues will be essential. Novel designs of mechanical strain sensors using fluorescence readouts such as FRET pairs and inventive imaging setups will be needed to fulfill these demands. Applying a repertoire of these approaches to a genetically tractable organism, such as *Dictyostelium* cells as they perform physiologically and medically important processes like cell division, will continue to provide unique insights into cellular mechanosensing and mechanotransduction.

Acknowledgements We are grateful to the insightful discussions and comments on the manuscript from Alexandra Surcel and Sheil Kee. We acknowledge the support of the National Institute of Health (Grant #GM066817) and the American Cancer Society (Grant #RSG CCG-114122).

Glossary List

Affine	Describes an actin network, which is co-linear during stretching and shearing
Non-affine	Describes an actin network in which co-linearity is absent during stretching and shearing
Stress	The force applied on a unit area
Strain	The ratio between the length-change associated with deformation and the original length (no deformation)
ABD	Actin-binding domain
ABP	Actin-binding protein
ACLP	Actin-crosslinking protein
BTF	Bipolar thick filament
ELC	Essential light chain
FJC	Free-joint-chain
HMM	Heavy meromyosin
RLC	Regulatory light chain
WLC	Worm-like-chain
D	Bundle size
E	Young's modulus: the proportionality between stress and the resulting strain
f_b	Bending modulus: the proportionality between bending momentum and the resulting curvature
G^*	Complex modulus
G'	Shear modulus – the real part of G^*: the proportionality between shear stress and the shear strain
G''	Loss modulus – the imaginary part of G^*
K'	Differential shear modulus: the differential proportionality between shear stress and the shear strain
L_c	Contour length: the integrated length along the polymer chain
L_p	Persistence length: the length over which correlations in the direction of the tangent are lost
L_e	Distance between entanglements
ξ	Mesh size
ς	Crosslinking density: the ratio between the cross-linker concentration and actin concentration

References

Ackbarow T, Chen X, Keten S, Buehler MJ (2007) Hierarchies, multiple energy barriers, and robustness govern the fracture mechanics of α-helical and β-sheet protein domains. Proc Natl Acad Sci USA 104:16410–16415

Addae-Mensah KA, Wikswo JP (2008) Measurement techniques for cellular biomechanics in vitro. Exp Biol Med 233:792–809

Altmann SM, Grünberg RG, Lenne PF, Ylänne J, Raae A, Herbert K, Saraste M, Nilges M, Hörber JK (2002) Pathways and intermediates in forced unfolding of spectrin repeats. Structure 10:1085–1096

Balaban NQ, Schwarz US, Riveline D, Goichberg P, Tzur G, Sabanay I, Mahalu D, Safran S, Bershadsky A, Addadi L, Geiger B (2001) Force and focal adhesion assembly: a close relationship studied using elastic micropatterned substrates. Nat Cell Biol 3: 466–472

Bañuelos S, Saraste, M, Djinović-Caruga K (1998) Structural comparisons of calponin homology domains: implications for actin binding. Structure 6:1419–1431

Bao G, Suresh S (2003) Cell and molecular mechanics of biological materials. Nat Mater 2: 715–725

Bausch AR, Kroy K (2006) A bottom-up approach to cell mechanics. Nat Phys 2:231–238

Beach JR, Egelhoff TT (2009) Myosin II recruitment during cytokinesis independent of centralspindlin-mediated phosphorylation. J Biol Chem 284:27377–27383

Bell GI (1978) Models for the specific adhesion of cells to cells. Science 200:618–627

Bertz M, Wilmanns M, Rief M (2009) The titin-telethonin complex is a directed, superstable molecular bond in the muscle Z-disk. Proc Natl Acad Sci USA 106:13307–133310

Boldogh I, Vojtov N, Karmon S, Pon LA (1998) Interaction between mitochondria and the actin cytoskeleton in budding yeast requires two integral mitochondrial outer member proteins, Mmm1p and Mdm10p. J Cell Biol 141:1371–1381

Brakebusch C, Fässler R (2003) The integrin-actin connection, an eternal love affair. EMBO J 22:2324–2333

Brangwynne CP, Koenderink GH, MacKintosh FC, Weitz DA (2009) Intracellular transport by active diffusion. Trends Cell Biol 19(9):423–427

Brockwell DJ, Paci E, Zinober RC, Beddard GS, Olmsted PD, Smith DA, Perham RN, Radford SE (2003) Pulling geometry defines the mechanical resistance of a β-sheet protein. Nat Struct Biol 10:731–737

Buchsbaum RJ (2007) Rho activation at a glance. J Cell Sci 120:1149–1152

Bueche F (1962) Physical properties of polymers 37. Interscience, New York, NY

Buehler MJ, Keten S (2008) Ealsticity, strength and resilience: a comparative study on mechanical signatures of α-helix, β-sheet and tropocollagen domains. Nano Research 1:63–71

Bursac P, Lenormand G, Fabry B, Oliver M, Weitz DA, Viasnoff V, Butler JP, Fredberg JJ (2005) Cytoskeletal remodelling and slow dynamics in the living. Nat Mater 4:557–561

Bustamante C, Marko JF, Siggia ED, Smith S (1994) Entropic elasticity of lambda-phage DNA. Science 265:1599–1600

Buxton GA, Clarke N (2007) "Bending to stretching" transition in disordered networks. Phys Rev Lett 98:238103–238106

Carrion-Vazquez M, Li H, Lu H, Marszalek P, Oberhauser AF, Fernandez JM (2003) The mechanical stability of ubiquitin is linkage dependent. Nat Struct Biol 10:738–743

Chaudhuri O, Parekh SH, Fletcher DA (2007) Reversible stress softening of actin network. Nature 445:295–298

Chen TL, Kowalczyk PA, Ho G, Chisholm RL (1995) Targeted disruption of the *Dictyostelium* myosin essential light chain gene produces cells defective in cytokinesis and morphogenesis. J Cell Sci 108:3207–3218

Chen Y, Yan B, Chalovich JM, Brenner B (2001) Theoretical kinetic studies of models for binding myosin subfragment-1 to regulated actin: Hill model versus Geeves model. Biophys J 80: 2338–2349

Chien S (2007) Mechanotransduction and endothelial cell homeostasis: the wisdom of the cell. Am J Physiol Heart Circ Physiol 292:H1209–H1224

Claessens MM, Bathe M, Frey E, Bausch AR (2006a) Actin-binding proteins sensitively mediate F-actin bundle stiffness. Nat Mater 5:748–753

Claessens MM, Tharmann R, Kroy K, Bausch AR (2006b) Microstructure and viscoelasticity of confined semiflexible polymer networks. Nat Phys 2:186–189

Craig R, Smith R, Kendrick-Jones J (1983) Light-chain phosphorylation controls the conformation of vertebrate non-muscle and smooth muscle myosin molecules. Nature 302:436–439

Crocker JC, Valentine MT, Weeks ER, Gisler T, Kaplan PD, Yodh AG, Weitz DA (2000) Two-point microrheology of inhomogeneous soft materials. Phys Rev Lett 85:888–891

Das M, MacKintosh FC, Levine AJ (2007) Effective medium theory of semiflexible filamentous networks. Phys Rev Lett 99:038101–038104

del Álamo JC, Norwich GN, Li YS, Lasheras JC, Chien S (2008) Anisotropic rheology and directional mechanotransduction in vascular endothelial cells. Proc Natl Acad Sci USA 105:15411–15416

del Rio A, Perez-Jimenez R, Liu R, Roca-Cusachs R, Fernandez JM, Sheetz MP (2009) Stretching single talin rod molecules activates vinculin binding. Science 323:638–641

Deng L, Trepat X, Butler JP, Millet E, Morgan KG, Weitz DA, Fredberg JJ (2006) Fast and slow dynamics of the cytoskelton. Nat Mater 5:636–640

Dietz H, Berkemeier F, Bertz M, Rief M (2006) Anisotropic deformation response of single protein molecules. Proc Natl Acad Sci USA 103:12724–12728

Djinović-Carugo K, Young P, Gautel M, Saraste M (1999) Structure of the alpha-actinin rod: molecular basis for cross-linking of actin-filaments. Cell 98:537–546

Effler JC, Kee YS, Berk JM, Tran, MN, Iglesias, PA, Robinson DN (2006) Mitosis-specific mechanosensing and contractile-protein redistribution control cell shape. Curr Biol 16: 1962–1967

Esue O, Tseng Y, Wirtz D (2009) α-Actinin and filamin cooperatively enhance the stiffness of actin filament networks. PLoS One 4:e4411

Evans E (2001) Probing the relation between force-lifetime-and chemistry in single molecular bonds. Annu Rev Biophys Biomol Struct 30:105–128

Evans E, Ritchie K (1997) Dynamic strength of molecular adhesion bonds. Biophys J 72: 1541–1555

Fabry B, Maksym GN, Butler JP, Glogauer M, Navajas D, Fredberg JJ (2001) Scaling the microrheology of living cells. Phys Rev Lett 87:148102–128105

Ferrer JM, Lee H, Chen J, Pelz B, Nakamura F, Kamm RD, Lang MJ (2008) Measuring molecular rupture forces between single actin filaments and actin-binding proteins. Proc Natl Acad Sci USA 105:9221–9226

Fettiplace R, Hackney CM (2006) The sensory and motor roles of auditory hair cells. Nat Rev Neurosci 7:19–29

Finer JT, Simmons RM, Spudich JA (1994) Single myosin molecule mechanics: piconewton forces and nanometre steps. Nature 368:113–119

Footer MJ, Kerssemakers JW, Theriot JA, Dogterom M (2007) Direct measurement of force generation by actin filament polymerization using an optical trap. Proc Natl Acad Sci USA 104:2181–2186

Forgacs G (1995) On the possible role of cytoskeletal filamentous networks in intracellular signaling: an approach based on percolation. J Cell Sci 108:2131–2143

Friedland JC, Lee MH, Boettiger D (2009) Mechanically activated integrin switch controls $\alpha_5\beta_1$ function. Science 323:642–644

Furuike S, Ito T, Yamazaki M (2001) Mechanical unfolding of single filamin A (ABP-280) molecules detected by atomic force microscopy. FEBS Lett 498:72–75

Gardel ML, Nakamura F, Hartwig JH, Crocker JC, Stossel TP, Weitz DA (2006) Prestressed F-actin networks cross-linked by hinged filamins replicate mechanical properties of cells. Proc Natl Acad Sci USA 103:1762–1767

Gardel ML, Shin JH, MacKintosh FC, Mahadevan L, Matsudaira P, Weitz DA (2004a). Elastic behavior of cross-linked and bundled actin networks. Science 304:1301–1305

Gardel ML, Shin JH, MacKintosh FC, Mahadevan L, Matsudaira PA, Weitz DA (2004b) Scaling of F-actin network rheology to probe single filament elasticity and dynamics. Phys Rev Lett 93:188102–188105

Gardel ML, Valentine MT, Crocker JC, Bausch AR, Weitz DA (2003) Microrheology of entangled F-actin solutions. Phys Rev Lett 91:158302–158305

Geiger B, Spatz JP, Bershadsky AD (2009) Environmental sensing through focal adhesions. Nat Rev Mol Cell Biol 10:21–33

Giannone G, Sheetz MP (2006) Substrate rigidity and force define form through tyrosine phosphatase and kinase pathways. Trends Cell Biol 16:213–223

Girard KD, Chaney C, Delannoy M, Kuo SC, Robinson DN (2004) Dynacortin contributes to cortical viscoelasticity and helps define the shape changes of cytokinesis. EMBO J 23: 1536–1546

Girard KD, Kuo SC, Robinson DN (2006) *Dictyostelium* myosin II mechanochemistry promotes active behavior of the cortex on long time scales. Proc Natl Acad Sci USA 103: 2103–2108

Gisler T, Weitz DA (1999) Scaling of the microrheology of semidilute F-actin solutions. Phys Rev Lett 82:1606–1609

Gittes F, Mickey B, Nettleton J, Howard J (1993) Flexural rigidity of microtubules and actin filaments measured from thermal fluctuations in shape. J Cell Biol 120:923–934

Gittes F, Schnurr B, Olmsted PD, MacKintosh FC, Schmidt CF (1997) Microscopic viscoelasticity: shear moduli of soft materials determined from the thermal fluctuations. Phys Rev Lett 79:3286–3289

Geeves MA, Halsall DJ (1987) Two-step ligand binding and cooperativity. A model to describe the cooperative binding of myosin subfragment 1 to regulated actin. Biophys J 52: 215–220

Guo B, Guilford WH (2006) Mechanics of actomyosin bonds in different nucleotide states are tuned to muscle contraction. Proc Natl Acad Sci USA 103:9844–9849

Head DA, Levine AJ, MacKintosh FC (2003) Deformation of cross-linked semiflexible polymer networks. Phys Rev Lett 91:108102–108105

Hill TL, Eisenberg E, Greene L (1980) Theoretical model for the cooperative equilibrium binding of myosin subfragment 1 to the actin-troponin-tropomyosin complex. Proc Natl Acad Sci USA 77:3186–3190

Hinner B, Tempel M, Sackmann E, Kroy K, Frey E (1998) Entanglement, elasticity, and viscous relaxation of actin solutions. Phys Rev Lett 81:2614–2617

Hoffman BD, Massiera G, van Citters KM, Crocker JC (2006) The consensus mechanics of cultured mammalian cells. Proc Natl Acad Sci USA 103:10259–10264

Holmes KC, Popp D, Gebhard W, Kabsch W (1990) Atomic model of the actin filament. Nature 347:44–49

Hostetter D, Rice S, Dean S, Altman D, McMahon PM, Sutton S, Tripathy A, Spudich JA (2004) *Dictyostelium* myosin bipolar thick filament formation: importance of charge and specific domains of the myosin rod. PLoS Biol 2:1880–1892

Howard J (2001) Mechanics of motor proteins and the cytoskeleton. Sinauer Associates, Sunderland, MA

Humphrey D, Duggan C, Saha D, Smith D, Käs J (2002) Active fluidization of polymer networks through molecular motors. Nature 416:413–416

Huveneers S, Danen EH (2009) Adhesion signaling-crosstalk between integrins, Src and Rho. J Cell Sci 122:1059–1069

Hynes RO (2002) Integrins: bidirectional, allosteric signaling machines. Cell 110:673–687

Ingber DE (2003) Tensegrity I: Cell structure and hierarchical systems. J Cell Sci 116:1157–1173

Ingber DE (2006) Cellular mechanotransduction: putting all the pieces together again. FASEB J 20:811–827

Izard T, Evans G, Borgon RA, Rush CL, Bricogne G, Bois PR (2004) Vinculin activation by talin through helical bundle conversion. Nature 427:171–175

Janmey PA, Hvidt S, Lamb J, Stossel TP (1990) Resemblance of actin-binding protein/actin gels to covalently crosslinked networks. Nature 345:89–92

Katsumi A, Naoe T, Matsushita T, Kaibuchi K, Schwartz MA (2005) Integrin activation and matrix binding mediate cellular response to mechanical stretch. J Biol Chem 280:16546–16549

Kaufmann S, Käs J, Goldmann WH, Sackmann E, Isenberg G (1992) Talin anchors and nucleates actin filaments at lipid membranes. A direct demonstration. FEBS Lett 314:203–205

Keten S, Buehler MJ (2008) Asymptotic strength limit of hydrogen-bond assemblies in proteins at vanishing pulling rates. Phys Rev Lett 100:198301–198304

Koenderink GH, Atakhorrami M, MacKintosh FC, Schmidt CF (2006) High-frequency stress relaxation in semiflexible polymer solutions and networks. Phys Rev Lett 96: 138307–138310

Koenderink GH, Dogic Z, Nakamura F, Bendix PM, MacKintosh FC, Hartwig JH, Stossel TP, Weitz DA (2009) An active biopolymer network controlled by molecular motors. Proc Natl Acad Sci USA 106:15192–15197

Kojima H, Ishijima A, Yanagida T (1994) Direct measurement of stiffness of single actin filaments with and without tropomyosin by in vitro nanomanipulation. Proc Natl Acad Sci USA 91:12962–12966

Kong F, García AJ, Mould AP, Humphries MJ, Zhu C (2009) Demonstration of catch bonds between an integrin and its ligand. J Cell Biol 185:1275–1284

Kovar DR, Pollard TD (2004) Insertional assembly of actin filament barbed ends in association with formins produces piconewton forces. Proc Natl Acad Sci USA 101:14725–14730

Kurpinski K, Chu J, Hashi C, Li S (2006) Anisotropic mechanosensing by mesenchymal stem cells. Proc Natl Acad Sci USA 103:16095–16100

Lau AW, Hoffman BD, Davies A, Crocker JC, Lubensky TC (2003) Microrheology, stress fluctuations, active behavior of living cells. Phys Rev Lett 91:198101–198103

Li H, Linke WA, Oberhauser AF, Carrion-Vazquez M, Kerkvilet JG, Lu H, Marszalek PE, Fernandez JM (2002) Reverse engineering of the giant muscle protein titin. Nature 418: 998–1002

Liang W, Warrick HM, Spudich JA (1999) A structural model for phosphorylation control of *Dictyostelium* myosin II thick filament assembly. J Cell Biol 147:1039–1048

Lieleg O, Bausch AR (2007) Cross-linker unbinding and self-similarity in bundled cytoskeletal networks. Phys Rev Lett 99:158105–158108

Lieleg O, Claessens MM, Heussinger C, Frey E, Bausch AR (2007) Mechanics of bundled semiflexible polymer networks. Phys Rev Lett 99:088102–088105

Lieleg O, Claessens MM, Luan Y, Bausch AR (2008) Transient binding and dissipation in cross-linked actin networks. Phys Rev Lett 101:108101–108104

Liu J, Koenderink GH, Kasza KE, MacKintosh FC, Weitz DA (2007) Visualizing the strain field in semiflexible polymer networks: strain fluctuations and nonlinear rheology of F-actin gels. Phys Rev Lett 98:198304–198307

Lu H, Schulten K (2000) The key event in force-induced unfolding of Titin's immunoglobulin domains. Biophys J 79:51–65

MacKintosh FC, Käs J, Janmey PA (1995) Elasticity of semiflexible biopolymer networks. Phys Rev Lett 75:4425–4428

Mahajan RK, Pardee JD (1996) Assembly mechanism of *Dictyostelium* myosin II: regulation by K^+, Mg^{2+}, actin filaments. Biochem 35:15504–15514

Marko JF, Siggia ED (1995) Stretching DNA. Macromolecules. 28:8759–8770

Martin SG, McDonald WH, Yates JR, Chang F (2005) Tea4p links microtubule plus ends with the formin for3p in the establishment of cell polarity. Dev Cell 8:479–491

Mizuno D, Tardin C, Schmidt CF, MacKintosh FC (2007) Nonequilibrium mechanics of active cytoskeletal networks. Science 315:370–373

Moffitt JR, Chemla YR, Smith SB, Bustamante C (2008) Recent advances in optical tweezers. Ann Rev Biochem 77:205–228

Moores SL, Spudich JA (1998) Conditional loss-of-myosin-II-function mutants reveal a position in the tail that is critical for filament nucleation. Mol Cell 1:1043–1050

Na S, Collin O, Chowdhury F, Tay B, Ouyang M, Wang Y, Wang N (2008) Rapid signal transduction in living cells is a unique feature of mechanotransduction. Proc Natl Acad Sci USA 105:6626–6631

Nebl T, Oh SW, Luna EJ (2000) Membrane cytoskeleton: PIP_2 pulls the strings. Curr Biol 10:R351–R354

Neuman KC, Nagy A (2008) Single-molecule force spectroscopy: optical tweezers, magnetic tweezers and atomic force microscopy. Nat Methods 5:491–505

Nome RA, Zhao JM, Hoff WD, Scherer NF (2007) Axis-dependent anisotropy in protein unfolding from integrated nonequilibrium single-molecule experiments, analysis, simulation. Proc Natl Acad Sci USA 104:20799–20804

Onck PR, Koeman T, van Dillen T, van der Giessen E (2005) Alternative explanation of stiffening in cross-linked semiflexible networks. Phys Rev Lett 95:178102–178105

Orlova A, Egelman EH (1997) Cooperative rigor binding of myosin to actin is a function of F-actin structure. J Mol Biol 265:469–474

Owen C, DeRosier D (1994) A 13-Å map of the actin-scruin filament from the limulus acrosomal process. J Cell Biol 123:337–344

Pascual J, Pfuhl M, Walther D, Saraste M, Nilges M (1997) Solution structure of the spectrin repeat: a left-handed antiparallel triple-helical coiled-coil. J Mol Biol 273: 740–751

Pelham RJ Jr, Wang Y (1997) Cell locomotion and focal adhesions are regulated by substrate flexibility. Proc Natl Acad Sci USA 94:13661–13665

Phichith D, Travaglia M, Yang Z, Liu X, Zong AB, Safer D, Sweeney HL (2009) Cargo binding induces dimerization of myosin VI. Proc Natl Acad Sci USA 106:17320–17324

Pollard TD (2007) Regulation of actin filament assembly by Arp2/3 complex and formins. Ann Rev Biophys Biomol Struct 36:451–477

Puklin-Faucher E, Sheetz MP (2009) The mechanical integrin cycle. J Cell Sci 122:179–186

Reichl EM, Ren Y, Morphew MK, Delannoy M, Effler JC, Girard KD, Divi S, Iglesias PA, Kuo SC, Robinson DN (2008) Interactions between myosin and actin crosslinkers control cytokinesis contractility dynamics and mechanics. Curr Biol 18:471–480

Ren Y, Effler JC, Norstrom M, Luo T, Firtel RA, Iglesias PA, Rock RS, Robinson DN (2009) Mechanosensing through cooperative interactions between myosin II and the actin crosslinker cortexillin I. Curr Biol 19:1421–1428

Revenu C, Athman R, Robine S, Louvard D (2004) The co-workers of actin filaments: from cell structure to signals. Nat Rev Mol Cell Biol 5:1–12

Rief M, Pascual J, Saraste M, Gaub HE (1999) Single molecule force spectroscopy of spectrin repeats: low unfolding forces in helix bundles. J Mol Biol 286:553–561

Riveline D, Zamir E, Balaban NQ, Schwarz US, Ishizaki T, Narumiya S, Kam Z, Geiger B, Bershadsky AD (2001) Focal contacts as mechanosensors: externally applied local mechanical force induces growth of focal contacts by an mDia1-dependent and ROCK-independent mechanism. J Cell Biol 153:1175–1186

Robinson DN, Spudich JA (2000) Towards a molecular understanding of cytokinesis. Trends Cell Biol 10:228–237

Robinson DN, Spudich JA (2004) Mechanics and regulation of cytokinesis. Curr Opin Cell Biol 16:182–188

Robling AG, Castillo AB, Turner CH (2006) Biomechanical and molecular regulation of bone remodeling. Annu Rev Biomed Eng 8:455–498

Rohs R, Etchebest C, Lavery R (1999) Unraveling proteins: a molecular mechanics study. Biophy J 76:2760–2768

Rosales-Nieves AE, Johndrow JE, Keller LC, Magie CR, Pinto-Santini DM, Parkhurst SM (2006) Coordination of microtubule and microfilament dynamics by *Drosophila* Rho1, spire and cappuccino. Nat Cell Biol 8:367–376

Rosenblatt J, Cramer LP, Baum B, McGee KM (2004) Myosin II-dependent cortical movement is required for centrosome separation and position during mitotic spindle assembly. Cell 117: 361–372

Sarkar A, Robertson RB, Fernandez JM (2004) Simultaneous atomic force microscope and fluorescence measurements of protein unfolding using a calibrated evanescent wave. Proc Natl Acad Sci USA 101:12882–12886

Sato N, Funayama N, Nagafuchi A, Yonemura S, Tsukita S, Tsukita S (1992) A gene family consisting of ezrin, radixin and moesin. Its specific localization at actin filament/plasma membrane association sites. J Cell Sci 103:131–143

Sawada Y, Tamada M, Dubin-Thaler BJ, Cherniavskaya O, Sakai R, Tanaka S, Sheetz MP (2006) Force sensing by mechanical extension of the src family kinase substrate p130Cas. Cell 127:015–1026

Schmidt CF, Bärmann M, Isenberg G, Sackmann E (1989) Chain dynamics, mesh size, and diffusive transport in networks of polymerized actin: a quasielastic light scattering and microfluorescence study. Macromolecules. 22:3638–3649

Schmoller KM, Lieleg O, Bausch AR (2008) Cross-linking molecules modify composite actin networks independently. Phys Rev Lett 101:118102–118105

Schwaiger I, Kardinal A, Schleicher M, Noegel AA, Rief M (2004) A mechanical unfolding intermediate in an actin-crosslinking protein. Nat Struct Mol Biol 11:81–85

Sechi AS, Wehland J (2000) The actin cytoskeleton and plasma membrane connection: Ptdlns(4,5)P_2 influences cytoskelton protein activity at the plasma membrane. J Cell Sci 113:3685–3695

Shin JH, Gardel ML, Mahadevan L, Matsudaira P, Weitz DA (2004) Relating microstructure to rheology of a bundled and cross-linked f-actin network in vitro. Proc Natl Acad Sci USA 101:9636–9641

Siegrist SE, Doe CQ (2007) Microtubule-induced cortical cell polarity. Genes Dev 21:483–496.

Sjöblom B, Ylänne J, Djinović-Carugo K (2008) Novel structural insights into F-actin-binding and novel functions of calponin homology domains. Curr Opin Struct Biol 18:702–708

Spudich JA (2001) The myosin swinging cross-bridge model. Nat Rev Mol Cell Biol 2:387–292

Stock A, Steinmetz MO, Janmey PA, Aebi U, Gerisch G, Kammerer RA, Weber I, Faix J (1999) Domain analysis of cortexillin I: actin-bundling, PIP_2-binding and the rescue of cytokinesis. EMBO J 18:5274–5284

Storm C, Pastore JJ, Mackintosh FC, Lubensky TC, Janmey PA (2005) Nonlinear elasticity in biological gels. Nature 435:191–194

Stossel TP, Fenteany G, Hartwig JH (2006) Cell surface actin remodeling. J Cell Sci 119: 3261–3264

Tadokoro S, Shattil SJ, Eto K, Tai V, Liddington RC, de Pereda JM, Ginsberg MH, Calderwood DA (2003) Talin binding to integrin beta tails: a final common step in integrin activation. Science 302:103–106

Tamada M, Sheetz MP, Sawada Y (2004) Activation of a signaling cascade by cytoskeleton stretch. Dev Cell 7:709–718

Tan JL, Tien J, Pirone DM, Gray DS, Bhadriraju K, Chen CS (2003) Cells lying on a bed of microneedles: an approach to isolate mechanical force. Proc Natl Acad Sci USA 100: 1484–1489

Tharmann R, Claessens MM, Bausch AR (2007) Viscoelasticity of isotropically cross-linked actin networks. Phys Rev Lett 98:088103–088106

Théry M, Bornens M (2006) Cell shape and cell division. Curr Biol 18:648–657

Thomas W (2008) Catch bond in adhesion. Ann Rev Biomed Eng 10:39–57

Tilghman RW, Parsons JT (2008) Focal adhesion kinase as a regulator of cell tension in the progression of cancer. Semin Cancer Biol 18:45–52

Tokuraku K, Kurogi R, Toya R, Uyeda TQ (2009) Novel mode of cooperative binding between myosin and Mg^{2+} -actin filaments in the presence of low concentrations of ATP. J Mol Biol 386:149–162

Trepat X, Deng L, An SS, Navajas D, Tschumperlin DJ, Gerthoffer WT, Butler J, Fredberg JJ (2007) Universal physical responses to stretch in the living cells. Nature 447:592–595

Tseng Y, Kole TP, Lee JS, Fedorov E, Almo SC, Schafer BW, Wirtz D (2005) How actin crosslinking and bundling proteins cooperate to generate an enhanced cell mechanical response. Biochem Biophys Res Comm 334:183–192

Tseng Y, Wirtz D (2001) Mechanics and multiple-particle tracking microheterogeneity of alpha-actinin-cross-linked actin filament networks. Biophys J 81:1643–1656

Tsuda Y, Yasutake H, Ishijima A, Yanagida T (1996) Torsional rigidity of single actin filaments and actin-actin bond breaking force under torsion measured directly by in vitro micromanipulation. Proc Natl Acad Sci USA 93:12937–12942

Uyeda TQ, Abramson PD, Spudich JA (1996) The neck region of the myosin motor domain acts as a lever arm to generate movement. Proc Natl Acad Sci USA 93:4459–4464

Vicente-Manzanares M, Choi CK, Horwitz AR (2009) Integrins in cell migration-the actin connection. J Cell Sci 122:199–206

Vogel V (2006) Mechanotransduction involving multimodular proteins: converting force into biochemical signals. Annu Rev Biophys Biomol Struct 35:459–488

Vogel V, Sheetz M (2006) Local force and geometry sensing regulate cell functions. Nat Rev Mol Cell Biol 7:265–275

Wachsstock DH, Schwartz WH, Pollard TD (1993) Affinity of α-Actinin for actin determines the structure and mechanical properties of actin filament gels. Biophys J 65:205–214

Wagner B, Tharmann R, Haase I, Fisher M, Bausch AR (2006) Cytoskeletal polymer networks: the molecular structure of cross-linkers determines macroscopic properties. Proc Natl Acad Sci USA 103:13974–13978

Wang CJ, Levchenko A (2009) Microfluidics technology for systems biology research. Methods Mol Biol 500:203–219

Wang N, Naruse K, Stamenovic D, Fredberg JJ, Mijailovich SM, Tolić-Nørrelykke IM, Polte T, Mannix R, Ingber DE (2001) Mechanical behavior in living cells consistent with the tensegrity model. Proc Natl Acad Sci USA 98:7765–7770

Wang N, Suo Z (2005) Long-distance propagation of forces in a cell. Biochem Biophys Res Comm 328:1133–1138

Wang N, Tytell JD, Ingber DE (2009) Mechanotransduction at a distance: mechanically coupling the extracellular matrix with the nucleus. Nat Rev Mol Cell Biol 10:75–82

Warrick HM, Spudich JA (1987) Myosin structure and function in cell motility. Ann Rev Cell Biol 3:379–427

Wilhelm C (2008) Out-of-equilibrium microrheology inside living cells. Phys Rev Lett 101:028101–028104

Wilhelm J, Frey E (2003) Elasticity of stiff polymer networks. Phys Rev Lett 91:108103–108106

Williamson JR (2008) Cooperativity in macromolecular assembly. Nat Chem Biol 4:458–465

Wirtz D (2009) Particle-tracking microrheology of living cells: principles and applications. Ann Rev Biophys 38:301–326

Zamir E, Geiger B (2001) Components of cell-matrix adhesions. J Cell Sci 114:3577–3579

Zhang W, Robinson DN (2005) Balance of actively generated contractile and resistive forces control cytokinesis dynamics. Proc Natl Acad Sci USA 102:7186–7191

Zhou EH, Trepat X, Park CY, Lenormand G, Oliver MN, Mijailovich SM, Hardin C, Weitz DA, Butler JP, Fredberg JJ (2009) Universal behavior of the osmotically compressed cell and its analogy to the colloidal glass transition. Proc Natl Acad Sci USA 106:10632–10637